From vacuole to cytosol – Disruptive invasion triggers cytosolic release of *Salmonella* Paratyphi A and subsequent cytosolic motility favors evasion of xenophagy

Felix Scharte[1], Rico Franzkoch[1, 2], Michael Hensel[1, 3]

ORCID: 0000-0002-6710-9524, FS; 0000-0002-8447-518X, RF; 0000-0001-6604-6253, MH

1 Abt. Mikrobiologie, Universität Osnabrück, Osnabrück, Germany

2 iBiOs - Integrated Bioimaging Facility Osnabrück

3 CellNanOs - Center of Cellular Nanoanalytics Osnabrück

Running title: Intracellular motile *S.* Paratyphi A evade xenophagy

Keywords: Typhoidal *Salmonella*, intracellular pathogen, autophagy, host cell invasion, pathogen-containing vacuole

Address for correspondence:

Michael Hensel

Abteilung Mikrobiologie

Fachbereich Biologie/Chemie, Universität Osnabrück

Barbarastr. 11

49076 Osnabrück, Germany

Tel: ++ 49 (0)541 969 3940

E-mail: Michael.Hensel@uni-osnabrueck.de

Abstract

Salmonella enterica is a common foodborne, facultative intracellular enteropathogen. Typhoidal *S. enterica* serovars like Paratyphi A (SPA) are human restricted and cause a severe systemic disease, while many *S. enterica* serovars like Typhimurium (STM) have broad host range, and in human hosts usually lead to self-limiting gastroenteritis. There are key differences between typhoidal and non-typhoidal *Salmonella* in pathogenesis, but underlying mechanisms remain largely unknown. Several genes encoding *Salmonella* pathogenicity island (SPI) effector proteins are absent or pseudogenes in SPA. Expression of virulence and metabolism genes show differential expression compared to STM. The intracellular transcriptomic architecture and phenotypes during presence in epithelial cells were recently described. Surprisingly, induction of motility, flagella and chemotaxis genes showed distinct expression patterns in intracellular SPA vs. STM and led to cytosolic motility of SPA. This study applies single cell microscopic analyses approaches to investigate the triggers and cellular consequences of cytosolic motility. Live cell imaging (LCI) revealed that SPA invades host cells in a highly cooperative manner. Extensive membrane ruffling at the invasion site leads to increased membrane damage in the nascent SCV with subsequent cytosolic release. After release into the cytosol, motile bacteria showed same velocity as under culture conditions used for infection. Reduced capture of SPA by autophagosomal membranes was observed by LCI and electron microscopy. Our results reveal flagella-mediated cytosolic motility as possible xenophagy evasion mechanism that could drive disease progression and contributes to dissemination of invasion-primed SPA during systemic infection.

46 **Importance**

47 Intracellular pathogens are commonly adapted to life in host cells either in a pathogen-containing
48 vacuole, or free in host cell cytosol. However, transitions between these lifestyles are possible and
49 demand specific adaptations, especially to avoid recognition and killing by host cell-autonomous
50 immune defense. *Salmonella enterica* serovar Paratyphi A (SPA) belongs to typhoidal *Salmonella*
51 able to cause live-threatening systemic infections in human hosts. We observed that SPA invades
52 host cells in a way that often results in damage of the nascent vacuole and release of SPA in host
53 cell cytosol. Here, SPA deploy flagella-mediated motility for rapid locomotion within infected
54 cells. We demonstrate on single cell level that flagella-mediated motility enables evasion of
55 xenophagic capture and control by the host cells. SPA uses a novel form of intracellular motility
56 to successfully colonize human host cells.

57

58 **Introduction**

59 Life inside mammalian host cells is a common virulence strategy of microbial pathogens and
60 various forms of adaptation to life within host cell cytosol or pathogen-containing vacuoles (PCV),
61 as well as exit strategies from host cells occur.

62 *Salmonella enterica* is a ubiquitous, invasive and facultative intracellular pathogen. Oral uptake of
63 *S. enterica* by contaminated food or water causes infectious diseases ranging from self-limiting
64 gastroenteritis to systemic infections with often fatal outcome (Dougan & Baker, 2014). While
65 non-typhoidal *Salmonella* (NTS) serovars, such as *S. enterica* serovar Typhimurium (STM) often
66 have broad host range, typhoidal *Salmonella* (TS) serovars such as *S*. Typhi (STY) or *S*. Paratyphi
67 A (SPA) are characterized by adaptation to primate hosts in which typhoid or paratyphoid fever
68 are important systemic diseases. The strict host adaptation limits studies of virulence mechanism
69 of TS, and frequently infection models of STM in susceptible mouse strains are used as surrogate
70 to investigate systemic *Salmonella* infections. However, SPA, STY and other TS are distinct from
71 NTS by presence of increased accumulation of pseudogenes (Holt et al., 2009; McClelland et al.,
72 2004), additional virulence factors as Vi capsule (STY) or typhoid toxin (STY, SPA), and distinct
73 regulation of expression of virulence functions (Cohen et al., 2022; Reuter et al., 2021).

74 Both NTS and TS invade non-phagocytic mammalian cells, such as epithelial cells, by trigger
75 invasion mediated by translocation of effector proteins by the *Salmonella* pathogenicity island 1
76 (SPI1)-encoded type III secretion system (T3SS). Host cell invasion is considered to initiate the
77 intracellular lifestyle of *Salmonella*, and allows to breach epithelial barriers. Translocation of SPI1-
78 T3SS effector proteins also evokes strong proinflammatory responses of epithelial cells, leading to
79 intestinal inflammation, a hallmark of gastroenteritis by NTS. While SPI1-T3SS also mediates
80 invasion by SPA and STY, intestinal inflammation usually is absent and other routes of entry

81 appear to be used to breach epithelial barriers of the intestines in order to reach systemic sites
82 (reviewed in Dougan & Baker, 2014).
83 Compiling data on the intracellular lifestyle in mammalian host cells reveal that STM is well-
84 adapted to life in specific PCV, referred to as *Salmonella*-containing vacuole, or SCV. The SCV
85 possesses canonical markers of late endosomal compartments, yet allows STM survival and
86 proliferation. The manipulation of the host cell endosomal system mainly mediated by effector
87 proteins of the SPI2-encoded T3SS is central to SCV formation and maintenance (Jennings et al.,
88 2017).
89 In addition to survival and proliferation in the SCV, further intracellular fates of STM are observed.
90 If the integrity of the SCV is not maintained, STM is exposed to host cell cytosol. This may evoke
91 xenophagic clearance, induce pyroptotic cell death, or may lead to cytosolic hyper-replication
92 resulting in release of highly infected enterocytes as observed for STM (Brumell et al., 2002;
93 Knodler et al., 2010).
94 In an approach to understand specific virulence mechanisms of TS, a comprehensive comparative
95 transcriptional analyses of intracellular STM and SPA was performed (Cohen et al., 2022). The
96 data revealed various differences in expression of metabolic functions and distinct patterns of
97 expression of flagella genes. We followed potential phenotypic consequences of the distinct
98 expression patterns and observed that a subpopulation of intracellular SPA expresses flagella and
99 is motile in host cell cytosol. Such flagella-mediated cytosolic motility was not observed for STM
100 present in host cell cytosol, and clearly is distinct from intracellular motility evolved by other
101 pathogens, where host cell actin polymerization is hijacked by various surface proteins.
102 Here we set out to analyze why SPA is released into cytosol, and how host cells respond to
103 intracellular motile SPA. In contrast to intracellular motility mediated by actin polymerization
104 (reviewed in Dowd et al., 2021), intracellular motility of SPA did not allow intercellular spread.

105 However, flagella-mediated motility enables SPA to avoid xenophagic clearance, as prerequisite
106 of host cell exit of invasion-primed motile SPA.
107

108 ## Results

109 **Early escape to host cell cytosol depends on invasion mechanism of SPA**

110 Although STM and SPA belong to the same species, the disease they cause in humans is very
111 different ranging from a self-limiting gastroenteritis in case of STM infection, to severe systemic
112 disease with potentially lethal outcome caused by SPA. We recently compared the intracellular
113 gene expression profiles of STM and SPA during infection and identified differences in the
114 expression of flagella/chemotaxis, SPI1, and carbon utilization pathways, and demonstrated
115 flagella-mediated movement of SPA in cytosol of host cell (Cohen et al., 2022). Flagella-mediated
116 motility was not observed for intracellular STM, despite a small proportion of STM also enters
117 host cell cytosol.

118 To further investigate phenotypic heterogeneity of intracellular SPA, we performed live cell
119 imaging (LCI) of infected LAMP1-GFP expressing HeLa cells, and compared SPA WT to isogenic
120 mutant strains deficient in flagella synthesis (Δ*fliC*), torque generation (Δ*motAB*), or certain
121 effector proteins of SPI1-T3SS (Δ*sopE*, Δ*sopE2*) or SPI2-T3SS (Δ*sifA*) crucial for early and late
122 SCV integrity. Furthermore, a SPA strain with a synthetic zipper invasion mechanism was
123 investigated, i.e. SPA Δ*invA* [P_{invF}::*Y.p. inv*] with defective SPI1-T3SS and *Yersinia*
124 *pseudotuberculosis* (*Y.p.*) Invasin protein Inv synthesized under control of SPI1 promoter P_{invF}.

125 We quantified the intracellular phenotypes in categories of 'cytosolic motile' and 'cytosolic non-
126 motile', while 'other' includes SPA residing in an SCV or showing cytosolic hyper-replication
127 (**Fig. 1**). In line with previous findings (Cohen et al., 2022), in about 38% of SPA WT-infected
128 host cells harbored cytosolic SPA exhibiting intracellular motility, while in 5% of infected cells
129 cytosolic SPA WT were non-motile (**Fig. 1AB**). SPA mutant strains with defects in maintaining
130 SCV integrity (Δ*sifA*), or lacking SPI1-T3SS effectors (Δ*sopE*, Δ*sopE2*) showed similar results of
131 phenotypes with cytosolic motile SPA Δ*sopE*, Δ*sopE2,* or Δ*sifA* in 30%, 39%, or 40 % of infected

132 cells, respectively. This population was absent in cells infected with non-motile mutant strains
133 lacking the flagella filament subunit FliC (**Fig. 1A** and **Fig. 1C**), or defective in energizing flagella
134 rotation (Δ*motAB*), similar to cells exposed to the antibiotics cefotaxime and ciprofloxacin
135 affecting bacterial cell wall synthesis and DNA replication during infection. Because Δ*motAB* and
136 Δ*fliC* strains are non-motile, we also tested if motility during invasion may affect intracellular
137 phenotypes. For this, expression of *motAB* was placed under control of promoter P_{tetA}, and induced
138 by addition of anhydrotetracycline (AHT) (Schulte et al., 2019). We induced expression of *motAB*
139 with AHT in bacterial culture and omitted AHT during infection and the following incubation time
140 to avert motility in infected HeLa cells. SPA Δ*motAB* [P_{tetA}*::motAB*] showed increased invasion
141 compared to Δ*motAB* (**Fig. S 4**), but also completely lacked the cytosolic motile subpopulation.
142 Further, we set out to evaluate the contribution of the mode of invasion to cytosolic release and
143 subsequent intracellular motility using mutant strain Δ*invA* incapable of translocation of trigger
144 invasion-mediating SPI1-T3SS effectors. We introduced a plasmid for expression of *Y.p. inv* under
145 control of SPI1 promoter P_{invF}, allowing expression under similar conditions as the SPI1-T3SS,
146 and therefore conferring zipper invasion to SPA. Interestingly, for this strain the subpopulation of
147 cytosolic motile bacteria was highly reduced to 1% of infected cells, the cytosolic subpopulation
148 was almost absent (5%), and SPA predominantly residing in SCV (**Fig. 1A** and **Fig. 1D**). These
149 data confirm previously data stating trigger invasion as driving force for cytosolic release (Röder
150 & Hensel, 2020).

151 **Cooperative trigger invasion of SPA leads to increased membrane damage of SCV**

152 It was previously described that the mode of trigger invasion and also strain-specific equipment
153 with SPI1-T3SS effectors affect cytosolic release following host cell entry and that trigger invasion
154 is often cooperative between *Salmonella* (Lorkowski et al., 2014; Röder & Hensel, 2020). We set
155 out to investigate membrane ruffling during invasion by LCI of different STM serovars and SPA

156 WT as well as SPA invading through zipper mechanism (**Fig. 2**, **Fig. S 1, Movie 1, Movie 2, Movie**
157 **3, Movie 4**). We observed rather small membrane ruffling for STM NCTC 12023 (**Fig. 2A**, **Fig. S**
158 **1, Movie 1**) and more extensive membrane ruffling for STM SL1344 (**Fig. 2B**, **Fig. S 1, Movie 2**).
159 Prolonged and extensive membrane ruffling of a larger cell area was observed for SPA WT (**Fig.**
160 **2C**, **Fig. S 1, Movie 3**). SPA Δ*invA* [P_{invF} *Y.p. inv*] showed lowest actin rearrangement at the
161 invasion site (**Fig. 2D**, **Fig. S 1, Movie 4**). Image analysis of foci of invasion indicated that STM
162 NCTC 12023 entry occurs mostly by single bacteria at invasion sites (mean = 1.6 STM cells per
163 site), whereas during the invasion of STM SL1344 multiple bacteria were involved in the process
164 (mean = 3.2 STM cells per site). SPA WT showed highest accumulation of bacteria at sites of
165 membrane rearrangement (mean = 7.3 SPA cells per site), but numbers were far lower when SPA
166 invaded through zipper mechanism (mean = 2.1 SPA cells per site).

167 **Trigger invasion enhances membrane damage at nascent SCVs**

168 Previous work revealed that the SCV is prone to rupture, and damages compartments are targeted
169 by membrane damage sensors and repair mechanisms such as galectins, sphingomyelinases, or the
170 ESCRT machinery (Ellison et al., 2020; Göser et al., 2020; Paz et al., 2010; Thurston et al., 2012).
171 We used an engineered version of equinatoxin II (EqtSM) as rapid membrane damage reporter that
172 is binding cytosol-exposed sphingomyelin in damages endosomal membranes (Deng et al., 2016;
173 Niekamp et al., 2022). HeLa cells expressing Halo-tagged EqtSM were infected by SPA WT or
174 SPA Δ*invA* [P_{invF}::*Y.p. inv*] to assess contribution of invasion mechanism to membrane damage of
175 the nascent SCV (**Fig 3**). LCI revealed that trigger invasion by SPA WT led to 45% of SCV positive
176 for EqtSM indicating transient membrane damage, while only 14% of SCV were EqtSM-positive
177 if SPA invaded through zipper mechanism (**Fig 3D**). The results underline the critical role of entry
178 mechanism for SCV integrity, and for subsequent intracellular lifestyle of *Salmonella*.
179

180 **Motility of cytosolic SPA interferes with xenophagic clearance**

181 A subset of intracellular pathogens such as *Listeria monocytogenes* (*L.m.*) or *Shigella flexneri*
182 actively escape the early PCV. As the host cell cytosol is a hostile environment for cytosolic
183 bacteria, e.g. due to recognition and clearance by cell-autonomous defense mechanism such as the
184 autophagosomal machinery, these pathogens evolved sophisticated defense mechanisms to avoid
185 decoration and degradation by expression of proteins interfering and inhibiting xenophagy. Such
186 mechanisms have not been reported for cytosolic *Salmonella*. An event preceding autophagic
187 clearance of cytosolic bacteria is ubiquitylation of their surface structures, such as LPS (Otten et
188 al., 2021). We also observed ubiquitylation of SPA located in host cell cytosol (**Fig. S 2**), and
189 analyzed if subsequent xenophagic clearance occurs. Alternatively, we hypothesized that cytosolic
190 motility of SPA may possibly interfere with xenophagy. To investigate on single cell level the
191 capture of SPA by autophagosomal membranes, we deployed late-autophagosomal membrane
192 protein LC3B as marker, generated a HeLa line stably expressing LC3B-GFP, and used this cell
193 line for infection by SPA and LCI. Individual intracellular SPA were scored for motility and
194 association with LC3B-positive membranes (**Fig. 4**, **Movie 5**, **Movie 6**). We compared SPA WT
195 to SPA Δ*motAB* [P_{tetA}::*motAB*] (motile during infection, but no intracellular motility), and SPA WT
196 treated with cefotaxime and ciprofloxacin (non-motile and non-replicative) regarding levels of
197 LC3B decoration. SPA-infected cells showed heterogenous populations as representative images
198 in **Fig. 4D-F** illustrate. The number of bacteria and also the degree of LC3B decoration varied from
199 cell to cell (**Fig. 4D-F**, **Movie 5**, **Movie 6**).

200 Image analysis of more than 170 infected cells with over 1,200 bacteria per condition (**Fig. 4A**,
201 **Fig. 4B**) revealed that residing in SCV efficiently avoids LC3B decoration for all strains (4.5%
202 LC3B-positive SPA WT, 5.7% LC3B-positive SPA Δ*motAB* [P_{tetA}::*motAB*]), with the highest rate
203 of LC3B decoration observed in cefo/cipro-treated SPA WT (9% LC3B-positive, **Fig. 4C**),

204 possibly due to failure of maintaining SCV integrity due to antibiotics treatment. However, the
205 cytosolic populations of the respective strains showed significant differences regarding LC3B
206 decoration. The enteric cytosolic population of SPA WT showed about 41.5% LC3B-positive
207 bacteria, whereas cytosolic populations of SPA Δ*motAB* [P_{tetA}::*motAB*], and SPA WT + cefo/cipro
208 both showed a high frequency of LC3B decoration (70.6%, 79.7%, respectively, **Fig. 4C**). We next
209 dissected the cytosolic population into groups of non-motile SPA and motile SPA to analyze effects
210 of motility on xenophagic escape. Surprisingly, SPA WT showed a high frequency of LC3B
211 decoration for the non-motile subpopulation (87.7%), but low frequency for the motile
212 subpopulation (18.6%). In contrast, the motile fraction was almost absent for SPA Δ*motAB*
213 [P_{tetA}::*motAB*] and SPA WT + cefo/cipro strains with only 31 and 8 counted bacteria, respectively
214 (**Fig. 4B**). Thus, the frequency of LC3B decoration of the cytosolic population of these strains
215 reflects that of the non-motile fraction with 71.1% and 80.2%, respectively. We conclude that
216 cytosolic motility is a major factor for xenophagic escape of SPA.
217 To further investigate the heterogenous fate of individual intracellular SPA subpopulations,
218 correlative light and electron microscopy (CLEM) analyses were performed to reveal ultrastructure
219 and membrane association (**Fig. 5**). Light microscopy allowed identification of cytosolic motile
220 and non-motile, as well as SCV-bound SPA for subsequent analyses by transmission electron
221 microscopy (TEM). Whereas cytosolic motile SPA showed no contact to membranous structures,
222 we observed SCV harboring SPA with distinct single membrane compartment in close contact to
223 the bacterial envelope (**Fig. 5D, E**). Cytosolic non-motile SPA showed association with LC3B-
224 positive membranes (**Fig. 5F**). The LC3B signal correlated double membrane structures
225 characteristic for autophagosomes. We also detected SPA that were partially enclosed by LC3B-
226 positive membranes, indicating either ongoing autophagosomal capture, or futile xenophagy.

227

228 **Increasing LC3B decoration hinders motility of cytosolic SPA**

229 For many bacteria of various cell shapes, flagellar rotation provides force for locomotion in their
230 habitat. The rotation of one or multiple flagellar filaments is thereby mediating phases of straight
231 swimming, alternating with phases of tumbling allowing orientation in chemical gradients. We set
232 out to investigate the maximum velocity of flagella-mediated movement of cytosolic SPA. As
233 previously demonstrated for multiple other bacteria, swimming speed is dependent on type of
234 flagellation and rotation speed of the flagellum (reviewed in Wadhwa & Berg, 2022). First, we
235 compared maximum velocity during different growth conditions in LB medium (**Fig. 6A**). SPA
236 cultures grown under aerobic conditions showed a median maximum velocity of 11 $\mu m\ s^{-1}$ when
237 grown overnight and 42 $\mu m\ s^{-1}$ when grown for 3.5 h while SPI1-inducing microaerophilic
238 conditions led to a median maximum velocity of 26 $\mu m\ s^{-1}$. Other intracellular pathogens such as
239 *L.m*. utilize actin polymerization to energize locomotion in host cell cytosol. We observed median
240 maximum velocity of cytosolic *L.m*. of 0.5 $\mu m\ s^{-1}$ (**Fig. 6**B) which was within the range of
241 previously published data (Lacayo & Theriot, 2004). In contrast, cytosolic SPA were able to move
242 almost as fast as SPA grown in media under microaerophilic conditions (25 $\mu m\ s^{-1}$; **Fig. 6C**).
243 As described above, a subpopulation of LC3B-decorated SPA was still able of movement (**Fig. 4**,
244 **Movie 5**, **Movie 6**). We hypothesized that increased autophagosomal capture delimits intracellular
245 motility of SPA, or in turn, intracellular motility prevents autophagosomal capture. To test these
246 possible correlations, we determined the signal intensity of SPA-associated LC3B-GFP as proxy
247 of degree of autophagosomal capture of individual SPA, and determined by tracking of the same
248 cytosolic SPA cells the maximum velocity (Fig. 6**D,** Fig. S 3). Plotting LC3B-GFP signal intensity
249 vs. maximal velocity of individual SPA indicated that velocity decreases with increasing
250 association with autophagosomal membranes. Linear regression with principal component analysis
251 showed a negative slope ($y=-19.5x + 21.9$) with maximum velocity, dropping to $<5\ \mu m\ s^{-1}$ at a

252 relative LC3B-GFP fluorescence of 0.86 which reflects an almost complete enclosure of SPA. We
253 conclude that flagella-mediated cytosolic motility of SPA counteracts host cell xenophagy.
254

255 **Discussion**

256 Our study investigated the causes of the recently described cytosolic motility of SPA (Cohen et al.,
257 2022) and its contributions to intracellular lifestyle. We demonstrated that mode of invasion and
258 equipment with SPI1-T3SS effector proteins is substantial for membrane damage at the nascent
259 SCV membrane and cytosolic release in early stage of infection. Furthermore, we showed that non-
260 motile SPA are targeted by autophagosomal membranes, However, the population of cytosolic
261 motile SPA is able to delay or escape xenophagic clearance as infection progresses. Our work adds
262 flagella-mediated motility of intracellular bacteria to the mechanisms of evasion of host cell
263 xenophagy.

264 The main findings of this study are summarized in **Fig 7**. We propose that release of SPA into
265 cytosol occurs early after invasion, and is likely due to the inability to generate a stable nascent
266 SCV (**Fig 7E**). We frequently observed clusters of invading SPA that induce high levels of local
267 actin recruitment, and extensive membrane ruffles. Such events likely lead to incomplete SCV
268 formation, and may allow clusters of bacteria to directly enter cytosol. This early exit from a labile
269 nascent SCV occurs so rapid that the transcriptional profile cannot be adjusted to the SCV-specific
270 repression of SPI1 and flagella regulons. We propose that a large proportion of intracellular SPA
271 maintains the transcriptional profile of invading bacteria. This hypothesis may be tested by
272 labelling of flagella, infection, and live cell imaging to follow the fate of flagella on SPA single
273 cells after invasion.

274 SPA possesses both SopE and SopE2. We previously demonstrated that STM harboring SopE2 and
275 SopE induce more severe membrane ruffles compared to the majority of STM strains only
276 harboring SopE2 (Röder & Hensel, 2020). The more overt trigger invasion by SopE-positive STM
277 was associated with increased cytosolic release, also occurring early after invasion. This may be
278 similar to damage of nascent SCV induced by SPA. However, we did not observe flagella-mediated

279 intracellular motility of SopE/SopE2-positive STM SL1344 (Cohen et al., 2022), indicating further
280 differences between STM and SPA. SPA possesses functional *sopE* and *sopE2*, while STY strains
281 possess functional *sopE* and pseudogenic *sopE2* (Valenzuela et al., 2015), thus damage of nascent
282 SCV after invasion of STY may be less pronounced compared to SPA.
283 A further factor possible contributing to decreased stability of the nascent SCV is the altered
284 function of SptP, a SPI1-T3SS effector protein with activity antagonistic to SopE. Prior work
285 showed that host cells fail to restore normal actin cytoskeleton organization when SptP is defective
286 and SopE activity overrules (Kubori & Galan, 2003). Recent work by Johnson *et al*. (Johnson et
287 al., 2017) demonstrated that SptP in STY and SPA have several AA exchanges that affect the
288 binding of chaperone SicP, and by this the efficiency of translocation.
289 Virtually all intracellular bacterial or parasitic pathogens adapted to cytosolic lifestyle have
290 convergently evolved mechanisms to recruit host cell G-actin for polar polymerization to F-actin,
291 resulting in actin-based motility (ABM) (reviewed in Dowd et al., 2021). ABM enables cell-to-cell
292 spread, and thus enables infection of new host cells without demanding exit and exposure to
293 antimicrobial mechanisms acting on extracellular bacteria. We did not observe intercellular spread
294 of SPA. While ABM is slower compared to flagella-mediated cytosolic motility of SPA, the higher
295 force generated by actin polymerization leads to generation of membrane protrusions and
296 ultimately to intercellular spread. Furthermore, switching between swimming and tumbling
297 motility restricts generation of membrane protrusions that are productive in infection of
298 neighboring cells. Yet, we have to consider that the applied model of confluently cultured non-
299 polarized epithelial cells may not reflect host cell types relevant during infection of human hosts
300 as main host cells of SPA are phagocytic cells, leading to dissemination through the lymphatic
301 system and further colonization of internal organs such as the liver, spleen, bone marrow and gall
302 bladder. Motility of SPA inside phagocytic cell line U937 has only been observed in spacious

303 vacuoles rather than in the cytosol of host cells (Cohen et al., 2022), probably because presence of
304 bacteria in cytosol of phagocytic cells most likely results in inflammatory cell death, so-called
305 pyroptosis (Castanheira & Garcia-Del Portillo, 2017). Similar observations were made for STM in
306 gallbladder epithelium (Knodler et al., 2010). In contrast to STM, SPA shows a lower replication
307 rate in host cells (Reuter et al., 2021). Defects in metabolic utilization of nutrients in host cell
308 cytosol such as glucose-6-phosphate and amino acids, and low SPI2-mediated replication inside
309 SCV may contribute to reduced replication numbers of intracellular SPA (Cohen et al., 2022; Forest
310 et al., 2010; Holt et al., 2009).
311 The cytosolic presence of pathogens such as *L. monocytogenes* or *S. flexneri* induce host cell-
312 intrinsic defense mechanisms, resulting in ubiquitination and xenophagy. Xenophagy is partially
313 avoided by ABM (Yoshikawa et al., 2009), but additional mechanisms appear required to
314 efficiently avoid autophagosomal degradation. These include the T3SS effector protein IcsB of *S.*
315 *flexneri* (Ogawa et al., 2005) with an acyltransferase activity affecting small GTPases and
316 membrane fusion machinery (Liu et al., 2018), or secreted Listeriolysin O and phospholipases of
317 *L. monocytogenes* targeting autophagosomal membranes (Birmingham et al., 2007). For SPA, the
318 high speed of flagella-mediated motility is sufficient to enable protection of a subpopulation of
319 cytosolic SPA against xenophagy (**Fig 7F**). Xenophagic clearance of cytosolic SPA is likely an
320 arms race between host cell and pathogen. If the autophagosomal machinery is rapidly delivered
321 to SPA and its flagella filament, motility is stopped and autophagy can be completed before SPA
322 motility and proliferation initiates (**Fig 7G**). The mode of trigger invasion by clusters of SPA, and
323 resulting simultaneous cytosolic presence of several SPA cells likely contributes to rapid
324 exhaustion of xenophagic capacity of the host cell, and inability to control SPA proliferation.
325 We showed that the cytosolic population is escaping xenophagic clearance by flagella-based
326 motility. Motile bacteria showed same maximum velocity in host cell cytosol as in culture media,

327 interfering with decoration by autophagosomal membranes, although cytosolic bacteria are already
328 ubiquitylated. If decoration by LC3B-positive membranes is only delayed to late time points of
329 infection and if this also leads to lysosomal degradation of engulfed bacteria deserves further
330 investigation. For several *Yersinia* strains it was reported that degradation by fusion with lysosomes
331 is inhibited and *Yersinia* is able to replicate in a non-acidic autophagosome (Connor et al., 2018;
332 Lemarignier & Pizarro-Cerda, 2020; Moreau et al., 2010; Straley & Harmon, 1984). Further
333 investigations assessing acidification of LC3B-positive compartments and interfering with
334 autophagosome formation using Lysotracker, siRNA approaches, and autophagy inhibitors such as
335 3-MA in combination with replication assays could help to understand the host-pathogen
336 interactions in SPA in more detail.
337 During systemic infections by TS induction of massive inflammatory response due to bacteria-
338 induced extrusion of infected cells which and not observed ad this is considered to contribute to
339 stealth strategy of TS (reviewed in Dougan & Baker, 2014; Hiyoshi, Tiffany, et al., 2018). Certain
340 features of immune evasion, such as avoidance of neutrophil oxidative burst have convergently
341 evolved, i.e. by expression of Vi capsule (STY) or the very long O-antigen of LPS (SPA) (Hiyoshi,
342 Wangdi, et al., 2018). Flagella-mediated intracellular motility has not been reported for STY, and
343 we did not observe increased numbers of cytosolic STY, nor detected flagella expressed by
344 intracellular STY. Functional flagella are expressed by intracellular *Legionella pneumophila*
345 during transition from the replicative to non-replicative, transmissive forms, and a recent study
346 showed that flagellated subpopulations emerge in the *Legionella*-containing vacuole (Schell et al.,
347 2016; Striednig et al., 2021). This transition occurs at the end of the intracellular replication cycle,
348 and stimulates host cell pyroptotic death, and release of *L. pneumophila* for new rounds of host cell
349 infection (Schell et al., 2016). We did not observe induction of host cell death by cytosolic motile
350 SPA, but this host cell response is highly cell type dependent. Further understanding of

351 physiological consequences of intracellular motility of SPA demand analyses in improved infection
352 models such as organoids of human origin (Sepe et al., 2020) that are capable to simulate tissues
353 closely related to *in vivo* conditions.
354

355 Acknowledgements

356 We thank Ohad Gal-Mor (Tel HaShomer, Israel) and the members SalHostTrop consortium
357 (InfectEra 3) for fruitful discussions on intracellular lifestyle of SPA and other TS. We thank Hans-
358 Peter Schmitz (Div. Genetics, UOS) for help with FACS of HeLa-LC3B-GFP cells. *Listeria*
359 *monocytogenes* expressing RFP was kindly provided by Martin Loessner (ETH Zürich). This work
360 was supported by the DFG through grant HE1964/23-1 as part of priority program SPP 2225 'Exit
361 strategies', and SFB 944 project Z.
362

363 ## Materials and Methods

364 *Bacterial strains and growth conditions*

365 In this study, *Salmonella enterica* serovar Typhimurium (STM) NCTC 12023, STM SL1344 and
366 *S. enterica* serovar Paratyphi A (SPA) 45157 were used as wild-type (WT) strains. All mutant
367 strains are isogenic to the respective WT and **Table 1** shows the characteristics. STM and SPA
368 strains were routinely cultured at 37 °C on Luria-Bertani (LB) agar or in LB broth using a roller
369 drum at 60 rpm. *Listeria monocytogenes* was grown on brain heart infusion (BHI) agar or in BHI
370 broth using a roller drum at 60 rpm. Antibiotics for maintenance of plasmids listed in **Table 2** were
371 added to LB in concentrations of 50 µg x ml^{-1} carbenicillin, 50 µg x ml^{-1} kanamycin, or 12 µg x
372 ml^{-1} chloramphenicol.

373 *Generation of bacterial strains*

374 Isogenic mutant strains were generated by λ Red recombineering for insertion of kanamycin
375 resistance (*aph*) cassettes amplified from template plasmids pKD4 or pKD13 as described before
376 (Chakravortty et al., 2002; Datsenko & Wanner, 2000) using oligonucleotides listed in **Table S1**.
377 Insertion of *aph* cassettes was confirmed by colony PCR. If required, the *aph* cassette was removed
378 by introduction of pE-FLP for FLP-mediated recombination.

379 *Construction of plasmids*

380 Plasmids were generated by Gibson assembly as described before (Röder et al., 2021; Röder &
381 Hensel, 2020; Schulte et al., 2019) using oligonucleotides listed in **Table S1**. Plasmids used in this
382 study are listed in **Table 2** and were introduced into the respective strains by electroporation.

383 *Host cell culture and infection*

384 Host cells were cultured and infected as described previously (Cohen et al., 2021). In short, HeLa
385 cells (ATCC no. CCL-2) were seeded in surface-treated 8-well chambered coverslips (ibidi) 24 or

386 48 h prior to infection to reach ~80% confluency (~80,000 cells) and were then used for infection.
387 Cells were continuously maintained in high glucose (4.5 g x l^{-1}) DMEM (Merck) supplemented
388 with 10% inactivated fetal calf serum (iFCS, Sigma) at 37 °C in a humidified atmosphere with 5%
389 CO_2. If indicated, cells were pulse-chased with 100 µg x ml^{-1} fluid phase marker Dextran
390 AlexaFluor 647 (Thermo Fisher Scientific) 16 h prior infection. STM strains for infection
391 experiments were subcultured from an overnight culture (1:31) in fresh LB medium and grown for
392 3.5 h at 37 °C under aerobic conditions using a roller drum at 60 rpm. SPA strains for infection
393 were grown for 8 h under aerobic conditions as described above and subcultured (1:100) in fresh
394 LB medium and stationary phase subcultures were grown for 16 h under microaerophilic conditions
395 as described in (Elhadad, Desai, et al., 2015). For infection with *Listeria monocytogenes*, overnight
396 cultures grown under aerobic conditions were used. Bacteria were adjusted to an optical density of
397 0.2 at 600 nm in PBS and used for infection with the respective MOI (between 5 and 90, dependent
398 on strain and experiment). Bacteria were centrifuged onto the cells for 5 min at 500 x *g* to
399 synchronize infection and incubated for 25 min. After washing thrice with PBS, cells were
400 incubated in medium containing 100 µg x ml^{-1} of gentamicin to kill extracellular bacteria.
401 Afterwards, cells were maintained in medium containing 10 µg x ml^{-1} gentamicin until fixation or
402 LCI. To image invasion of *Salmonella* into HeLa cells, cells were infected directly on microscope
403 stage and imaged for ~1 h.

404 *Generation of HeLa cells stably expressing LC3B::GFP*

405 HeLa cells stably expressing LC3B-GFP were generated using 3rd generation lentiviral vectors and
406 subsequent fluorescence-activated cell sorting (FACS) (Broad, 2015; Institute, 2015; TRC, 2015a,
407 2015b). Supernatant containing lentivirus was generated by seeding 3.8 x 10^5 cells x ml^{-1} HEK
408 293FT cells (Invitrogen R700-07) in 10 cm tissue culture plates (10 ml per plate, TPP) in antibiotic-
409 free growth media (high glucose DMEM + 10% iFCS). After 24 h, cells should be 70-80%

410 confluent and were then transfected with lentiviral packaging plasmid (9 µg psPAX2), envelope
411 plasmid (0.9 µg pMD2.G) and pLX304 carrying eGFP-LC3B (9 µg) using Opti-MEM (Fisher
412 Scientific) and FuGENE HD transfection reagent (Promega). Transfection mix was incubated for
413 30 min at room temperature before added to cells dropwise. Cells were incubated for at least 18 h
414 and medium was changed to 15 ml growth medium containing 30% iFCS. Medium containing
415 lentivirus was harvested after 24 h and 48 h and centrifuged at 350 x *g* for 5 min to pellet any
416 residual packaging cells. Supernatant was stored in sterile polypropylene storage tubes and stored
417 at -80 °C. Half of the harvested supernatant was filtered using fast flow & low binding filters
418 (Merck Millipore).
419 HeLa cells were seeded in 24-well plates (1 x 10^5 cells x ml^{-1}) and incubated for 24 h before 8 µg
420 x ml^{-1} Polybrene (Sigma) was added to the cells. Filtered supernatant containing lentivirus was
421 added to cells 48 h after seeding. 48 h after lentivirus was added to cells, medium was exchanged
422 to DMEM containing 10 µg x ml^{-1} Blasticidin (Invitrogen) and incubated for 72 h. Medium was
423 changed to DMEM without antibiotics to allow growth for 24 h before cells were detached for
424 culture in tissue culture flasks (TPP) to obtain sufficient cells numbers for FACS.
425 For FACS of lentivirus transfected HeLa cells, cells were detached from tissue culture flask and
426 resuspended in appropriate amount of medium to reach concentration of 1 x 10^7 cells x ml^{-1}. A 100
427 µm cell strainer (BD Falcon) was used to prevent aggregation of cells prior to FACS. Cells were
428 sorted for GFP fluorescence with BD FACS Aria. A mixed population of cells with different GFP
429 expression levels was obtained. GFP-positive cells were cultured again in tissue culture flasks
430 before a second round of FACS with Sony SH800S was conducted. Single cells were sorted into
431 96-well plates to obtain single clones of LC3B-GFP expressing cells. Cell clones were analyzed
432 regarding GFP intensity, cell division, and phenotypes of intracellular *Salmonella* prior to use in
433 further experiments.

434 *Live cell imaging (LCI)*

435 Prior to LCI, medium of infected HeLa cells was changed to high glucose DMEM without phenol
436 red supplemented with 30 mM HEPES. LCI was performed at 37 °C and an atmosphere of 5% CO_2
437 with Cell Observer microscope (Zeiss) equipped with Yokogawa Spinning Disc Unit CSU
438 X1a5000, an incubation chamber, 63x objective (α-Plan-Apochromat, NA 1.46) and 40x objective
439 (Plan-Apochromat, NA 1.4), two ORCA Flash 4.0 V3 cameras (Hamamatsu) and appropriate
440 filters for the respective fluorescence proteins or dyes.

441 *Correlative light and electron microscopy (CLEM)*

442 CLEM of HeLa LC3B-GFP infected by SPA was performed as previously described (Krieger et
443 al., 2014). Briefly, HeLa LC3B-GFP cells were grown on MatTek dishes with gridded coverslips.
444 Cells were fixed with 4% paraformaldehyde (Electron Microscopy Sciences) and 0.1%
445 glutaraldehyde (Electron Microscopy Sciences) in 200 mM HEPES directly on microscope stage
446 during imaging of cytosolic motile SPA. Cells were incubated for 30 min and were then rinsed
447 thrice with 200 mM HEPES buffer. Cells were subsequently fixed with 2.5% glutaraldehyde in
448 200 mM HEPES for 1 h, washed thrice with buffer and post-fixed with 2% osmium-tetroxide
449 (Electron Microscopy Sciences), 0.1% ruthenium red (Applichem) and 1.5% potassium
450 ferrocyanide (Sigma) in 200 mM HEPES on ice. After several washing steps, the cells were
451 dehydrated in a cold graded series of ethanol and finally one rinse in anhydrous ethanol and two
452 rinses in anhydrous acetone at room temperature. Infiltration was performed with increasing
453 concentrations of EPON812 (Sigma) in anhydrous acetone. Utilizing the coordinate system, the
454 ROI from light microscopy was relocated on the EPON block, trimmed and 70 nm serial sections
455 were cut with an ultramicrotome (Leica EM UC7, Leica, Wetzlar, Germany) and collected on
456 formvar-coated copper slot grids (Plano). Grids were post-stained for 30 min with 2% uranyl
457 acetate (Roth) and 20 min with 3% lead citrate (Leica). TEM images were acquired using a Zeiss

458 Leo 912 Omega (Zeiss, Oberkochen, Germany) equipped with a CCD camera (TRS, Moorenwies,
459 Germany). Overlays of the light and electron microscopic images were generated using LAS AF
460 (Leica) and Photoshop CS6 (Adobe).

461 *Tracking analyses*

462 For microscopic tracking analyses, bacterial cultures were imaged with Cell Observer microscope
463 (Zeiss) equipped with 100x objective (α-Plan-Apochromat, NA 1.46) and CoolSNAP camera at
464 about 8 frames per second (fps) over 1 min. For tracking of intracellular SPA, infected cells were
465 imaged with Cell Observer microscope (Zeiss) equipped with Yokogawa Spinning Disc Unit CSU
466 X1a5000, an incubation chamber, 63x objective (α-Plan-Apochromat, NA 1.46), two ORCA Flash
467 4.0 V3 cameras (Hamamatsu) and appropriate filters for the respective fluorescence proteins at
468 about 18 fps over 1 min. Tracking analyses were performed in Fiji with TrackMate v5.0.2 plugin
469 (Tinevez et al., 2017) with minimal displacement threshold of 1 µm. For tracking of intracellular
470 *L.m.*, infected cells were imaged with setup as described for intracellular SPA at ~0.1 fps over 10-
471 30 min. Tracking analyses were performed in FIJI with manual tracking plugin.

472 *Analyses of LC3B decoration*

473 For analyses of LC3B-decoration of intracellular SPA, randomly selected infected cells were
474 imaged 3-4 h p.i. as described above and were analyzed manually regarding LC3B-GFP signal at
475 SPA cell bodies. 100 µg x ml^{-1} cefotaxime and ciprofloxacin were added 2 h p.i. if indicated.
476 For correlation of maximum velocity and LC3B decoration of cytosolic SPA, individual bacteria
477 were analyzed regarding LC3B-GFP fluorescence intensity using ZEISS Efficient Navigation
478 (ZEN) software. Manual tracking with the same bacteria was performed as described above.

479 *Transfection of HeLa cells with Halo-tagged EqtSM*

480 HeLa cells were maintained and infected as described above. In short, cells were seeded in 8-wells
481 2 d prior infection. Cells were transfected with Halo-tagged EqtSM expression construct 1 d prior
482 infection using FuGENE HD in 1:2 ratio. Infected cells were labeled with 100 nM Janelia Fluor
483 646 HaloTag ligand (Promega, GA1120) for 30 min, washed five times with PBS and subsequently
484 imaged using the Zeiss Cell Observer SD microscope set-up.

485 **Suppl. Materials and Methods**

486 *Immuno-staining and fluorescence microscopy*

487 For immuno-staining of HeLa LAMP1-GFP cells infected by SPA, cells were seeded in 24-well
488 plates (TPP) on coverslips 24 h or 48 h prior infection to reach ~80% confluency (~180,000 cells).
489 Cultivation of bacteria and infection of HeLa cells was carried out as described above. Infected
490 cells were fixed with 3% PFA at the desired time point. After washing thrice with PBS, cells were
491 incubated in blocking solution (2% goat serum, 2% BSA, 0.1% saponin in PBS) for 30 min. Next,
492 cells were incubated for 1 h at RT with mouse monoclonal antibodies against Ubiquitin (Biomol
493 PW 8810). After washing cells thrice with PBS, cells were incubated with primary antibodies
494 against *Salmonella* O-Antigen of SPA (BD Difco 229471) for 1 h. After washing thrice with PBS,
495 cells were stained with the appropriate secondary antibodies for 1 h (Invitrogen A11031, Dianova
496 111-607-003). After three washing steps with PBS, coverslips were mounted with Fluoroshield
497 (Sigma) and sealed with Entellan (Merck). Microscopy of fixed samples was performed with Leica
498 SP5 confocal laser-scanning microscope using 100x objective (HCX PL APO CS, NA 1.4-0.7) and
499 polychroic mirror TD 488/543/633.

500 *Flow cytometry*

501 The assay was performed as described previously (Reuter et al., 2021). Briefly, HeLa cells were
502 seeded in 12-well plates (TPP) 48 h prior infection to reach confluency (~4 x 10^5 cells per well) on
503 the day of infection. Cells were infected with STM and SPA cultures at MOI 30 as described above.
504 The bacterial strains harbored fluorescence reporter plasmids. At 1 h and 3 h p.i., cells were washed
505 thrice with PBS, detached from culture plates, fixed with 3% PFA and analyzed by flow cytometry
506 using Attune NxT cytometer. At least 3,000 infected cells were measured and analyzed regarding
507 expression of fluorescence reporter.

508 *Gentamicin protection assays*

509 The assay was performed as described before (Kuhle & Hensel, 2002). Briefly, HeLa cells were
510 seeded in 24-well plates (TPP) 48 h prior infection to reach confluency (~2 x 10^5 cells per well) on
511 the day of infection. Cells were infected with STM and SPA cultures at MOI 5 as described above.
512 Cells were washed thrice with PBS and lysed using 0.1% Triton X-100 at 1 h and 16 h p.i. Colony
513 forming units were determined by plating serial dilutions of lysates and inoculum on Mueller-
514 Hinton II agar and incubated overnight at 37 °C. The percentage of internalized bacteria of the
515 inoculum (from subcultures) and the replication rate of intracellular bacteria was calculated.

516

517 **References**

518 Birmingham, C. L., Canadien, V., Gouin, E., Troy, E. B., Yoshimori, T., Cossart, P., Higgins, D.
519 E., & Brumell, J. H. (2007). *Listeria monocytogenes* evades killing by autophagy during
520 colonization of host cells. *Autophagy*, *3*(5), 442-451. https://doi.org/10.4161/auto.4450
521 Broad, I. (2015). *Lentivirus production of ShRNA, CRISPR, or ORF-pLX clones in 10 cm dishes*
522 *or 6-well plates* [TRC Laboratory Protocols].
523 https://portals.broadinstitute.org/gpp/public/resources/protocols
524 Brumell, J. H., Tang, P., Zaharik, M. L., & Finlay, B. B. (2002). Disruption of the *Salmonella*-
525 containing vacuole leads to increased replication of *Salmonella enterica* serovar
526 typhimurium in the cytosol of epithelial cells. *Infect Immun*, *70*(6), 3264-3270.
527 https://www.ncbi.nlm.nih.gov/pubmed/12011022
528 Castanheira, S., & Garcia-Del Portillo, F. (2017). *Salmonella* Populations inside Host Cells. *Front*
529 *Cell Infect Microbiol*, *7*, 432. https://doi.org/10.3389/fcimb.2017.00432
530 Chakravortty, D., Hansen-Wester, I., & Hensel, M. (2002). *Salmonella* pathogenicity island 2
531 mediates protection of intracellular *Salmonella* from reactive nitrogen intermediates. *J Exp*
532 *Med*, *195*(9), 1155-1166. https://doi.org/10.1084/jem.20011547
533 Cohen, E., Azriel, S., Auster, O., Gal, A., Zitronblat, C., Mikhlin, S., Scharte, F., Hensel, M.,
534 Rahav, G., & Gal-Mor, O. (2021). Pathoadaptation of the passerine-associated *Salmonella*
535 *enterica* serovar Typhimurium lineage to the avian host. *PLoS Pathog*, *17*(3), e1009451.
536 https://doi.org/10.1371/journal.ppat.1009451
537 Cohen, H., Hoede, C., Scharte, F., Coluzzi, C., Cohen, E., Shomer, I., Mallet, L., Holbert, S., Serre,
538 R. F., Schiex, T., Virlogeux-Payant, I., Grassl, G. A., Hensel, M., Chiapello, H., & Gal-
539 Mor, O. (2022). Intracellular *Salmonella* Paratyphi A is motile and differs in the expression
540 of flagella-chemotaxis, SPI-1 and carbon utilization pathways in comparison to intracellular
541 *S.* Typhimurium. *PLoS Pathog*, *18*(4), e1010425.
542 https://doi.org/10.1371/journal.ppat.1010425
543 Connor, M. G., Pulsifer, A. R., Chung, D., Rouchka, E. C., Ceresa, B. K., & Lawrenz, M. B. (2018).
544 *Yersinia pestis* Targets the Host Endosome Recycling Pathway during the Biogenesis of
545 the *Yersinia*-Containing Vacuole To Avoid Killing by Macrophages. *mBio*, *9*(1).
546 https://doi.org/10.1128/mBio.01800-17
547 Datsenko, K. A., & Wanner, B. L. (2000). One-step inactivation of chromosomal genes in
548 *Escherichia coli* K-12 using PCR products. *Proc Natl Acad Sci U S A*, *97*(12), 6640-6645.
549 https://doi.org/10.1073/pnas.120163297
550 Deng, Y., Rivera-Molina, F. E., Toomre, D. K., & Burd, C. G. (2016). Sphingomyelin is sorted at
551 the trans Golgi network into a distinct class of secretory vesicle. *Proc Natl Acad Sci U S A*,
552 *113*(24), 6677-6682. https://doi.org/10.1073/pnas.1602875113
553 Dougan, G., & Baker, S. (2014). *Salmonella enterica* serovar Typhi and the pathogenesis of
554 typhoid fever. *Annu Rev Microbiol*, *68*, 317-336. https://doi.org/10.1146/annurev-micro-
555 091313-103739
556 Dowd, G. C., Mortuza, R., & Ireton, K. (2021). Molecular Mechanisms of Intercellular
557 Dissemination of Bacterial Pathogens. *Trends Microbiol*, *29*(2), 127-141.
558 https://doi.org/10.1016/j.tim.2020.06.008
559 Drecktrah, D., Levine-Wilkinson, S., Dam, T., Winfree, S., Knodler, L. A., Schroer, T. A., &
560 Steele-Mortimer, O. (2008). Dynamic behavior of *Salmonella*-induced membrane tubules
561 in epithelial cells. *Traffic*, *9*(12), 2117-2129. https://doi.org/10.1111/j.1600-
562 0854.2008.00830.x

563 Elhadad, D., Desai, P., Rahav, G., McClelland, M., & Gal-Mor, O. (2015). Flagellin Is Required
564 for Host Cell Invasion and Normal *Salmonella* Pathogenicity Island 1 Expression by
565 *Salmonella enterica* Serovar Paratyphi A. *Infect Immun*, *83*(9), 3355-3368.
566 https://doi.org/10.1128/IAI.00468-15
567 Elhadad, D., McClelland, M., Rahav, G., & Gal-Mor, O. (2015). Feverlike Temperature is a
568 Virulence Regulatory Cue Controlling the Motility and Host Cell Entry of Typhoidal
569 *Salmonella*. *J Infect Dis*, *212*(1), 147-156. https://doi.org/10.1093/infdis/jiu663
570 Ellison, C. J., Kukulski, W., Boyle, K. B., Munro, S., & Randow, F. (2020). Transbilayer
571 Movement of Sphingomyelin Precedes Catastrophic Breakage of Enterobacteria-
572 Containing Vacuoles. *Curr Biol*, *30*(15), 2974-2983 e2976.
573 https://doi.org/10.1016/j.cub.2020.05.083
574 Forest, C. G., Ferraro, E., Sabbagh, S. C., & Daigle, F. (2010). Intracellular survival of *Salmonella*
575 *enterica* serovar Typhi in human macrophages is independent of *Salmonella* pathogenicity
576 island (SPI)-2. *Microbiology*, *156*(Pt 12), 3689-3698.
577 https://doi.org/10.1099/mic.0.041624-0
578 Gal-Mor, O., Suez, J., Elhadad, D., Porwollik, S., Leshem, E., Valinsky, L., McClelland, M.,
579 Schwartz, E., & Rahav, G. (2012). Molecular and cellular characterization of a *Salmonella*
580 *enterica* serovar Paratyphi a outbreak strain and the human immune response to infection.
581 *Clin Vaccine Immunol*, *19*(2), 146-156. https://doi.org/10.1128/CVI.05468-11
582 Gerlach, R. G., Claudio, N., Rohde, M., Jäckel, D., Wagner, C., & Hensel, M. (2008). Cooperation
583 of *Salmonella* pathogenicity islands 1 and 4 is required to breach epithelial barriers. *Cell*
584 *Microbiol*, *10*(11), 2364-2376. https://doi.org/10.1111/j.1462-5822.2008.01218.x
585 Göser, V., Kehl, A., Röder, J., & Hensel, M. (2020). Role of the ESCRT-III complex in controlling
586 integrity of the *Salmonella*-containing vacuole. *Cell Microbiol*, *22*(6), e13176.
587 https://doi.org/10.1111/cmi.13176
588 Hiyoshi, H., Tiffany, C. R., Bronner, D. N., & Baumler, A. J. (2018). Typhoidal *Salmonella*
589 serovars: ecological opportunity and the evolution of a new pathovar. *FEMS Microbiol Rev*,
590 *42*(4), 527-541. https://doi.org/10.1093/femsre/fuy024
591 Hiyoshi, H., Wangdi, T., Lock, G., Saechao, C., Raffatellu, M., Cobb, B. A., & Baumler, A. J.
592 (2018). Mechanisms to Evade the Phagocyte Respiratory Burst Arose by Convergent
593 Evolution in Typhoidal Salmonella Serovars. *Cell Rep*, *22*(7), 1787-1797.
594 https://doi.org/10.1016/j.celrep.2018.01.016
595 Hoffmann, S., Schmidt, C., Walter, S., Bender, J. K., & Gerlach, R. G. (2017). Scarless deletion of
596 up to seven methyl-accepting chemotaxis genes with an optimized method highlights key
597 function of CheM in *Salmonella* Typhimurium. *PLoS One*, *12*(2), e0172630.
598 https://doi.org/10.1371/journal.pone.0172630
599 Holt, K. E., Thomson, N. R., Wain, J., Langridge, G. C., Hasan, R., Bhutta, Z. A., Quail, M. A.,
600 Norbertczak, H., Walker, D., Simmonds, M., White, B., Bason, N., Mungall, K., Dougan,
601 G., & Parkhill, J. (2009). Pseudogene accumulation in the evolutionary histories of
602 *Salmonella enterica* serovars Paratyphi A and Typhi. *BMC Genomics*, *10*, 36.
603 https://doi.org/10.1186/1471-2164-10-36
604 Institute, T. R. C. T. B. (2015). Lentivirus production of ShRNA, CRISPR, or ORF-pLX clones in
605 10 cm dishes or 6-well plates [TRC Laboratory Protocols].
606 https://portals.broadinstitute.org/gpp/public/resources/protocols
607 Jennings, E., Thurston, T. L. M., & Holden, D. W. (2017). *Salmonella* SPI-2 Type III Secretion
608 System Effectors: Molecular Mechanisms And Physiological Consequences. *Cell Host*
609 *Microbe*, *22*(2), 217-231. https://doi.org/10.1016/j.chom.2017.07.009

610 Johnson, R., Byrne, A., Berger, C. N., Klemm, E., Crepin, V. F., Dougan, G., & Frankel, G. (2017).
611 The Type III Secretion System Effector SptP of *Salmonella enterica* Serovar Typhi. *J*
612 *Bacteriol*, *199*(4). https://doi.org/10.1128/JB.00647-16
613 Knodler, L. A., Vallance, B. A., Celli, J., Winfree, S., Hansen, B., Montero, M., & Steele-Mortimer,
614 O. (2010). Dissemination of invasive *Salmonella* via bacterial-induced extrusion of
615 mucosal epithelia. *Proc Natl Acad Sci U S A*, *107*(41), 17733-17738.
616 https://doi.org/10.1073/pnas.1006098107
617 Krieger, V., Liebl, D., Zhang, Y., Rajashekar, R., Chlanda, P., Giesker, K., Chikkaballi, D., &
618 Hensel, M. (2014). Reorganization of the endosomal system in *Salmonella*-infected cells:
619 the ultrastructure of *Salmonella*-induced tubular compartments. *PLoS Pathog*, *10*(9),
620 e1004374. https://doi.org/10.1371/journal.ppat.1004374
621 Kubori, T., & Galan, J. E. (2003). Temporal regulation of *Salmonella* virulence effector function
622 by proteasome-dependent protein degradation. *Cell*, *115*(3), 333-342. 14636560
623 Kuhle, V., & Hensel, M. (2002). SseF and SseG are translocated effectors of the type III secretion
624 system of *Salmonella* pathogenicity island 2 that modulate aggregation of endosomal
625 compartments. *Cell Microbiol*, *4*(12), 813-824. https://doi.org/10.1046/j.1462-
626 5822.2002.00234.x
627 Lacayo, C. I., & Theriot, J. A. (2004). *Listeria monocytogenes* actin-based motility varies
628 depending on subcellular location: a kinematic probe for cytoarchitecture. *Mol Biol Cell*,
629 *15*(5), 2164-2175. https://doi.org/10.1091/mbc.e03-10-0747
630 Lemarignier, M., & Pizarro-Cerda, J. (2020). Autophagy and Intracellular Membrane Trafficking
631 Subversion by Pathogenic *Yersinia* Species. *Biomolecules*, *10*(12).
632 https://doi.org/10.3390/biom10121637
633 Liu, W., Zhou, Y., Peng, T., Zhou, P., Ding, X., Li, Z., Zhong, H., Xu, Y., Chen, S., Hang, H. C.,
634 & Shao, F. (2018). N(epsilon)-fatty acylation of multiple membrane-associated proteins by
635 *Shigella* IcsB effector to modulate host function. *Nat Microbiol*, *3*(9), 996-1009.
636 https://doi.org/10.1038/s41564-018-0215-6
637 Lorkowski, M., Felipe-Lopez, A., Danzer, C. A., Hansmeier, N., & Hensel, M. (2014). *Salmonella*
638 *enterica* invasion of polarized epithelial cells is a highly cooperative effort. *Infect Immun*,
639 *82*(6), 2657-2667. https://doi.org/10.1128/IAI.00023-14
640 McClelland, M., Sanderson, K. E., Clifton, S. W., Latreille, P., Porwollik, S., Sabo, A., Meyer, R.,
641 Bieri, T., Ozersky, P., McLellan, M., Harkins, C. R., Wang, C., Nguyen, C., Berghoff, A.,
642 Elliott, G., Kohlberg, S., Strong, C., Du, F., Carter, J., . . . Wilson, R. K. (2004). Comparison
643 of genome degradation in Paratyphi A and Typhi, human-restricted serovars of *Salmonella*
644 *enterica* that cause typhoid. *Nat Genet*, *36*(12), 1268-1274. https://doi.org/10.1038/ng1470
645 Moreau, K., Lacas-Gervais, S., Fujita, N., Sebbane, F., Yoshimori, T., Simonet, M., & Lafont, F.
646 (2010). Autophagosomes can support *Yersinia pseudotuberculosis* replication in
647 macrophages. *Cell Microbiol*, *12*(8), 1108-1123. https://doi.org/10.1111/j.1462-
648 5822.2010.01456.x
649 Niekamp, P., Scharte, F., Sokoya, T., Vittadello, L., Kim, Y., Deng, Y., Südhoff, E., Hilderink, A.,
650 Imlau, M., Clarke, C. J., Hensel, M., Burd, C. G., & Holthuis, J. C. M. (2022). Ca^{2+}-
651 activated sphingomyelin scrambling and turnover mediate ESCRT-independent lysosomal
652 repair. *Nat Commun*, *13*(1), 1875. https://doi.org/10.1038/s41467-022-29481-4
653 Noster, J., Chao, T. C., Sander, N., Schulte, M., Reuter, T., Hansmeier, N., & Hensel, M. (2019).
654 Proteomics of intracellular *Salmonella enterica* reveals roles of *Salmonella* pathogenicity
655 island 2 in metabolism and antioxidant defense. *PLoS Pathog*, *15*(4), e1007741.
656 https://doi.org/10.1371/journal.ppat.1007741

Ogawa, M., Yoshimori, T., Suzuki, T., Sagara, H., Mizushima, N., & Sasakawa, C. (2005). Escape of intracellular *Shigella* from autophagy. *Science*, *307*(5710), 727-731. 15576571

Otten, E. G., Werner, E., Crespillo-Casado, A., Boyle, K. B., Dharamdasani, V., Pathe, C., Santhanam, B., & Randow, F. (2021). Ubiquitylation of lipopolysaccharide by RNF213 during bacterial infection. *Nature*, *594*(7861), 111-116. https://doi.org/10.1038/s41586-021-03566-4

Paz, I., Sachse, M., Dupont, N., Mounier, J., Cederfur, C., Enninga, J., Leffler, H., Poirier, F., Prevost, M. C., Lafont, F., & Sansonetti, P. (2010). Galectin-3, a marker for vacuole lysis by invasive pathogens. *Cell Microbiol*, *12*(4), 530-544. https://doi.org/10.1111/j.1462-5822.2009.01415.x

Reuter, T., Scharte, F., Franzkoch, R., Liss, V., & Hensel, M. (2021). Single cell analyses reveal distinct adaptation of typhoidal and non-typhoidal *Salmonella enterica* serovars to intracellular lifestyle. *PLoS Pathog*, *17*(6), e1009319. https://doi.org/10.1371/journal.ppat.1009319

Röder, J., Felgner, P., & Hensel, M. (2021). Comprehensive Single Cell Analyses of the Nutritional Environment of Intracellular *Salmonella enterica*. *Front Cell Infect Microbiol*, *11*, 624650. https://doi.org/10.3389/fcimb.2021.624650

Röder, J., & Hensel, M. (2020). Presence of SopE and mode of infection result in increased *Salmonella*-containing vacuole damage and cytosolic release during host cell infection by *Salmonella enterica*. *Cell Microbiol*, *22*(5), e13155. https://doi.org/10.1111/cmi.13155

Schell, U., Simon, S., & Hilbi, H. (2016). Inflammasome Recognition and Regulation of the *Legionella* Flagellum. *Curr Top Microbiol Immunol*, *397*, 161-181. https://doi.org/10.1007/978-3-319-41171-2_8

Schulte, M., Sterzenbach, T., Miskiewicz, K., Elpers, L., Hensel, M., & Hansmeier, N. (2019). A versatile remote control system for functional expression of bacterial virulence genes based on the *tetA* promoter. *Int J Med Microbiol*, *309*(1), 54-65. https://doi.org/10.1016/j.ijmm.2018.11.001

Sepe, L. P., Hartl, K., Iftekhar, A., Berger, H., Kumar, N., Goosmann, C., Chopra, S., Schmidt, S. C., Gurumurthy, R. K., Meyer, T. F., & Boccellato, F. (2020). Genotoxic Effect of *Salmonella* Paratyphi A Infection on Human Primary Gallbladder Cells. *mBio*, *11*(5). https://doi.org/10.1128/mBio.01911-20

Straley, S. C., & Harmon, P. A. (1984). *Yersinia pestis* grows within phagolysosomes in mouse peritoneal macrophages. *Infect Immun*, *45*(3), 655-659. https://doi.org/10.1128/iai.45.3.655-659.1984

Striednig, B., Lanner, U., Niggli, S., Katic, A., Vormittag, S., Brulisauer, S., Hochstrasser, R., Kaech, A., Welin, A., Flieger, A., Ziegler, U., Schmidt, A., Hilbi, H., & Personnic, N. (2021). Quorum sensing governs a transmissive *Legionella* subpopulation at the pathogen vacuole periphery. *EMBO Rep*, *22*(9), e52972. https://doi.org/10.15252/embr.202152972

Studer, P., Staubli, T., Wieser, N., Wolf, P., Schuppler, M., & Loessner, M. J. (2016). Proliferation of *Listeria monocytogenes* L-form cells by formation of internal and external vesicles. *Nat Commun*, *7*, 13631. https://doi.org/10.1038/ncomms13631

Thurston, T. L., Wandel, M. P., von Muhlinen, N., Foeglein, A., & Randow, F. (2012). Galectin 8 targets damaged vesicles for autophagy to defend cells against bacterial invasion. *Nature*, *482*(7385), 414-418. https://doi.org/10.1038/nature10744

Tinevez, J. Y., Perry, N., Schindelin, J., Hoopes, G. M., Reynolds, G. D., Laplantine, E., Bednarek, S. Y., Shorte, S. L., & Eliceiri, K. W. (2017). TrackMate: An open and extensible platform for single-particle tracking. *Methods*, *115*, 80-90. https://doi.org/10.1016/j.ymeth.2016.09.016

705 TRC. (2015a, June, 3 2015). *Lentivirus production of ShRNA, CRISPR, or ORF-pLX clones in 10*
706 *cm dishes or 6-well plates*. Retrieved July, 4 2022 from
707 https://portals.broadinstitute.org/gpp/public/resources/protocols
708 TRC. (2015b, June, 3 2015). *Lentivirus production of ShRNA, CRISPR, or ORF-pLX clones in 10*
709 *cm dishes or 6-well plates*. https://portals.broadinstitute.org/gpp/public/resources/protocols
710 Valenzuela, L. M., Hidalgo, A. A., Rodriguez, L., Urrutia, I. M., Ortega, A. P., Villagra, N. A.,
711 Paredes-Sabja, D., Calderon, I. L., Gil, F., Saavedra, C. P., Mora, G. C., & Fuentes, J. A.
712 (2015). Pseudogenization of *sopA* and *sopE2* is functionally linked and contributes to
713 virulence of *Salmonella enterica* serovar Typhi. *Infect Genet Evol*, *33*, 131-142.
714 https://doi.org/10.1016/j.meegid.2015.04.021
715 Wadhwa, N., & Berg, H. C. (2022). Bacterial motility: machinery and mechanisms. *Nat Rev*
716 *Microbiol*, *20*(3), 161-173. https://doi.org/10.1038/s41579-021-00626-4
717 Yoshikawa, Y., Ogawa, M., Hain, T., Yoshida, M., Fukumatsu, M., Kim, M., Mimuro, H.,
718 Nakagawa, I., Yanagawa, T., Ishii, T., Kakizuka, A., Sztul, E., Chakraborty, T., &
719 Sasakawa, C. (2009). *Listeria monocytogenes* ActA-mediated escape from autophagic
720 recognition. *Nat Cell Biol*, *11*(10), 1233-1240. https://doi.org/10.1038/ncb1967

721

722 **Tables:**

723 **Table 1**. Bacterial strains used in this study

Designation	Relevant characteristics	Reference
S. Typhimurium NCTC 12023 (ATCC 14028) (MvP)	wild type, *sopE2*	Lab collection
MvP503	Δ*sifA*::FRT	(Kuhle & Hensel, 2002)
MvP1890	Δ*ssaV*::FRT	(Noster et al., 2019)
MvP2769	Δ*uhpT*::*aph*	This study
MvP2801	Δ*uhpT*::FRT	This study
MvP818	Δ*invC*::FRT	(Gerlach et al., 2008)
S. Typhimurium SL1344	wild type, *sopE*, *sopE2*	Lab collection
S. Paratyphi A 45157 (SPA)	wild type, clinical isolate, Nepal outbreak in 2009	(Gal-Mor et al., 2012)
SPA146	Δ*sopE*::*aph*	This study
SPA147	Δ*sopE2*::*aph*	This study
SPA110	Δ*sifA*::*aph*	(Reuter et al., 2021)
SPA144	Δ*fliC*::FRT	(Cohen et al., 2022)
SPA145	Δ*motAB*::*aph*	This study
SPA *invA*	Δ*invA*::FRT	(Elhadad, McClelland, et al., 2015)
SPA *ssaR*	Δ*ssaR*::FRT	(Reuter et al., 2021)
Listeria monocytogenes EGD	EGDe::pPL2P$_{xyllong}$-Lm RFP	(Studer et al., 2016)

724

725 **Table 2**. Plasmids used in this study

Designation	Relevant characteristics	Reference
p3589	P_{rpsM}::mCherry, Cm^r	(Lorkowski et al., 2014)
pFPV-mCherry	P_{rpsM}::mCherry, $Carb^r$	(Drecktrah et al., 2008)
pKD4	template *aph* cassette	Datsenko and Wanner, 2000
pKD13	template *aph* cassette	Datsenko and Wanner, 2000
pWRG730	Red recombinase expression	(Hoffmann et al., 2017)
pMD2.G	2nd generation lentiviral packaging vector, $Carb^r$	Addgene #12259
psPAX2	VSV-G envelope expressing vector, $Carb^r$	Addgene #12260
p3776	P_{EM7}::RFP P_{ssaG}::sfGFP, $Carb^r$	(Röder & Hensel, 2020)
p5400	pLX304 eGFP::LC3B, 3rd generation lentivirus vector, $Carb^r$	This study, based on Addgene #25890
p4114	P_{invF}::*Y.p. inv,* $Carb^r$	(Röder & Hensel, 2020)
p4889	P_{EM7}::RFP P_{uhpT}::sfGFP, $Carb^r$	(Röder & Hensel, 2020)
p5212	STM *uhpABCT*, Kan^r	This study
p5387	P_{EM7}::mScarlet-I P_{sopE}::sfGFP, $Carb^r$	This study
p5776	EqtSMcyto::HaloTag in pLX304, $Carb^r$	This study, based on (Niekamp et al., 2022)
p5825	P_{sopE}::sfGFP::LVA, $Carb^r$	This study

p5833	P_{invF}::*Y.p. inv* P_{EM7}::tagRFP-T, Carb^r	This study
p6159	*tetR* P_{tetA}::*motAB*, Carb^r	This study

726

727 **Figures and figure legends:**

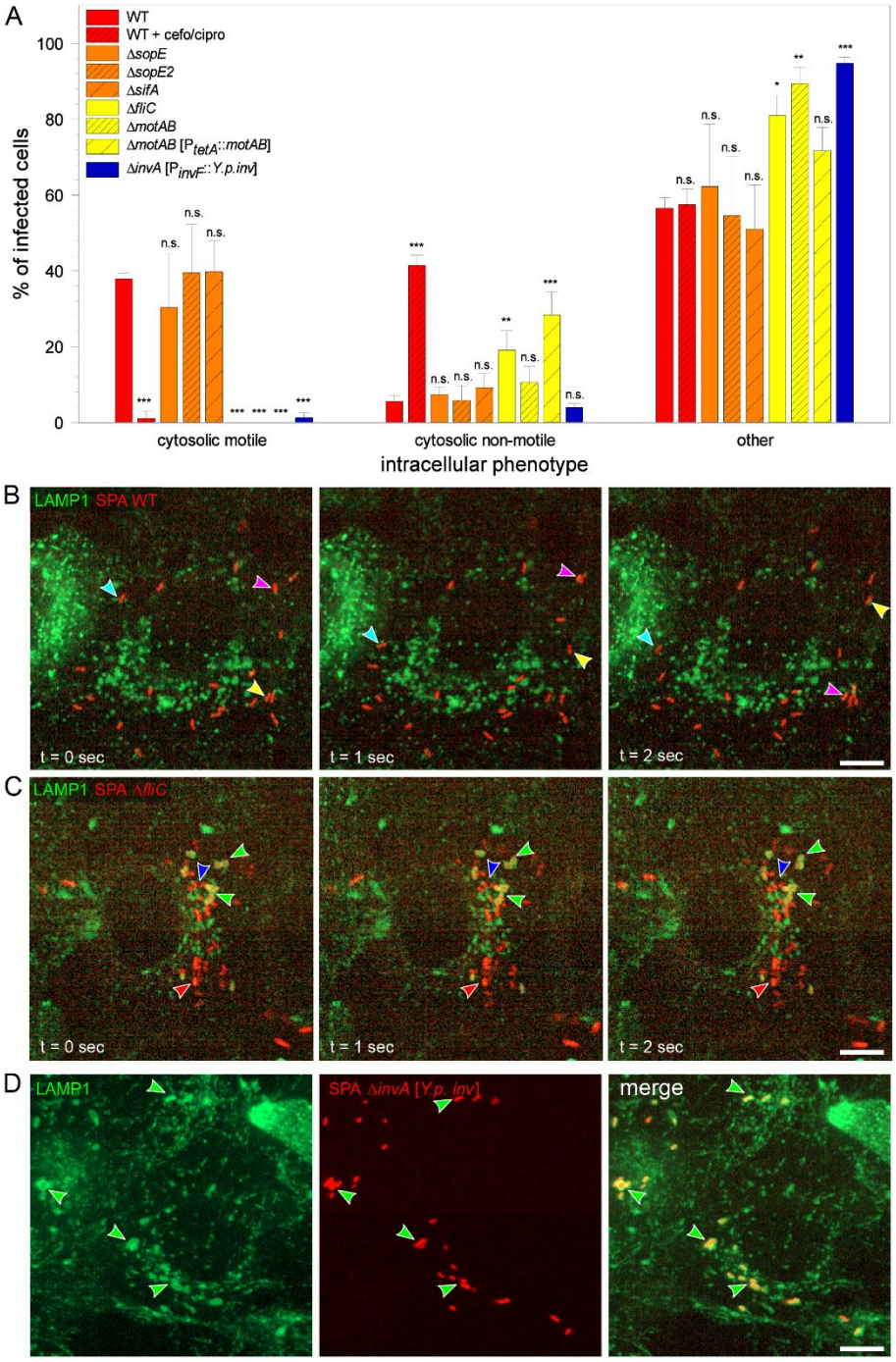

728

729 **Fig. 1**. **Quantification of intracellular SPA phenotypes**. **A-E.** HeLa cells stably expressing
730 LAMP1-GFP (green) were infected with *Salmonella* Paratyphi A (SPA) WT or isogenic mutant
731 strains expressing mCherry (red) at MOI 30, 60, or 90 for WT, Δ*invA* [P_{invF}::*Y.p. inv*], or Δ*fliC*,

732 Δ*motAB*, respectively. **A.** Quantification of intracellular phenotypes was performed during live cell
733 imaging. From 4-6 h p.i., at least 100 infected cells per strain were examined for intracellular
734 phenotypes. Data are means and standard deviations (SD) from three independent experiments.
735 Statistical analysis was performed with one-way ANOVA and is indicated as n.s., not significant;
736 *, $p < 0.05$; **, $p < 0.01$; ***, $p < 0.001$. **B, C.** Time-lapse images of infected HeLa-LAMP1-GFP
737 cells showing movement of three cytosolic SPA WT (**B**, turquoise, magenta and yellow
738 arrowhead), no movement of cytosolic SPA Δ*fliC* (**C**, red and blue arrowhead) and SPA Δ*fliC*
739 residing in SCV (**C**, green arrowheads). **D.** Maximum intensity projection of HeLa-LAMP1-GFP
740 cells infected with SPA Δ*invA* [P_{invF}::*Y.p. inv*] residing in SCV (green arrowheads). Scale bars: 10
741 µm.
742

743

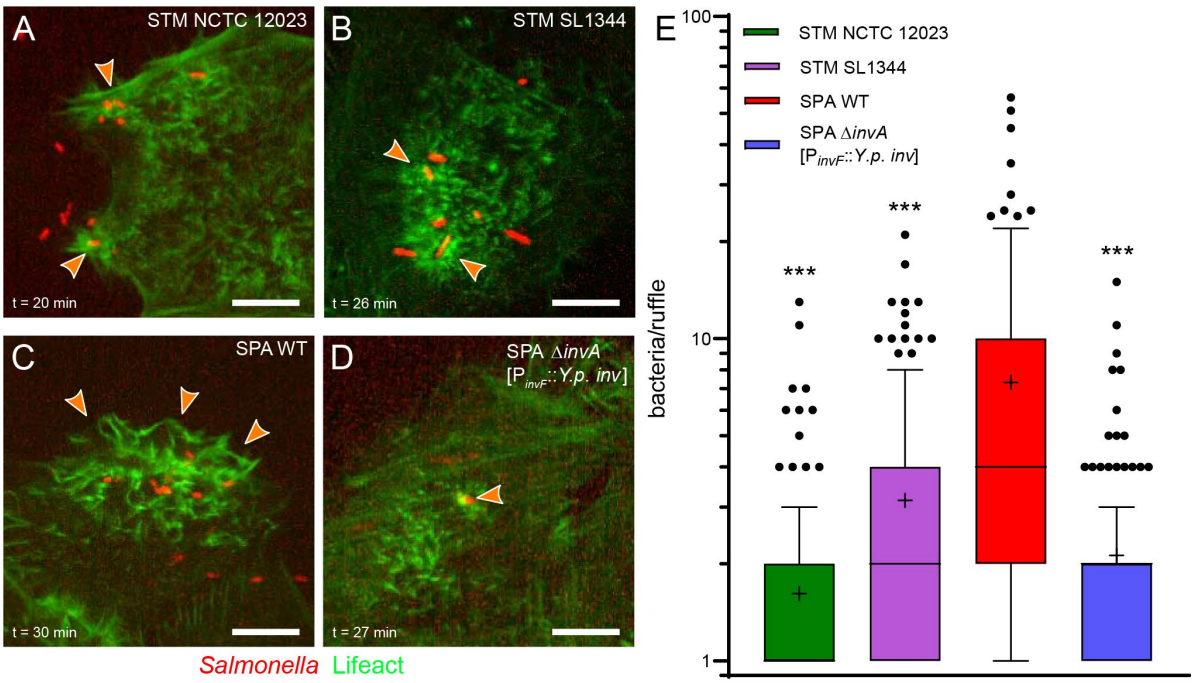

744 **Fig. 2**. **SPA induces massive membrane ruffles during trigger invasion, and invades in highly**
745 **cooperative manner. A-D.** HeLa cells stably expressing Lifeact-eGFP (green) were infected with
746 STM NCTC 12023 (**A**), STM SL1344 (**B**), SPA WT (**C**), or SPA Δ*invA* [P_{invF}::*Y.p. inv*] (**D**)
747 expressing mCherry (red) at MOI 75. Cells in chambered coverslips were infected on microscope
748 stage and imaged for 1 h by spinning disc confocal microscopy with intervals of 3-5 min between
749 images. Still images from time-lapse are shown. Arrowheads indicate sites of ongoing invasion.
750 Scale bars: 10 µm. **E.** Image series were assessed for numbers of invading bacteria per ruffle.
751 Shown are Tukey´s box plots of invading bacteria per ruffle during infection with error bars
752 including data of 1.5 x interquartile range (IQR). Outliers beyond the 1.5 x IQR are shown as dots.
753 Middle lines and "+" denote median and mean value, respectively. Compiled from three
754 independent experiments, 200, 169, 170, and 130 individual invasion events were analyzed for
755 STM NCTC 12023, STM SL1344, SPA WT, and SPA Δ*invA* [P_{invF}::*Y.p. inv*], respectively,.
756 Statistical analysis compared to SPA WT was performed with unpaired two-tailed t test and is
757 indicated as *** for $p < 0.001$.

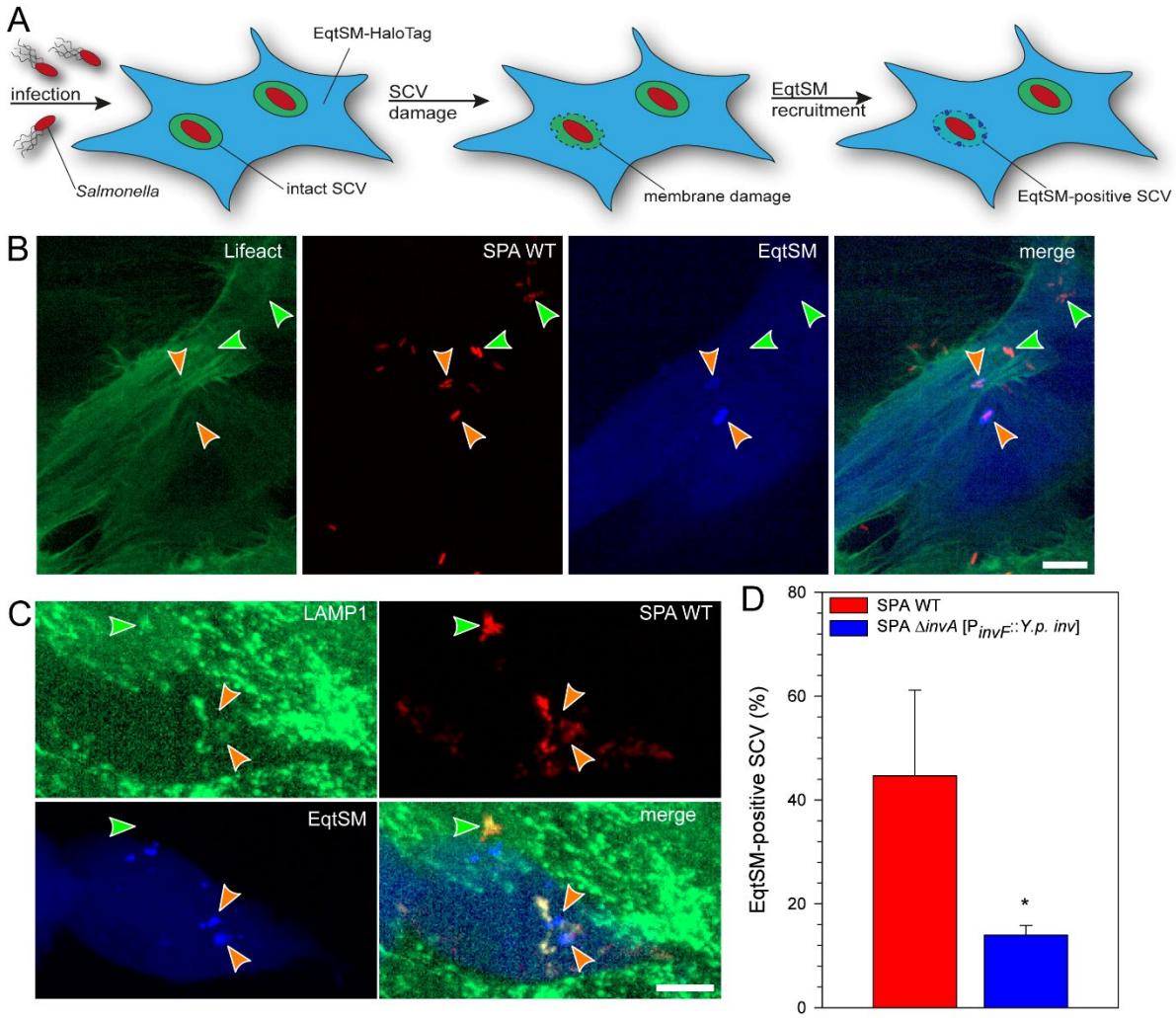

758

759 **Fig 3. Trigger invasion by SPA destabilizes nascent SCVs. A.** To localize sites of SPA-induced
760 membrane damage and to quantify the frequency of SCV damage, HeLa cells stably expressing
761 LAMP1-GFP (**B**) or Lifeact-eGFP (**C**) (green) were transfected for expression of EqtSM-HaloTag
762 and labeled with Janelia Fluor 646 HaloTag ligand (blue). Subsequently, cells were infected with
763 SPA WT or SPA Δ*invA* [P_{invF}::*Y.p. inv*] expressing mCherry (red). Infected cells were imaged 1-2
764 h p.i. and representative infected cells are shown as maximum intensity projection. Arrowheads
765 indicate intact SCVs (green), or SCVs targeted by EqtSM (orange). Scale bars: 10 µm. **D**. SCVs
766 were scored for association with EqtSM-HaloTag. Data are means and SD from three independent

767 experiments. Statistical analysis was performed with unpaired two-tailed t test and is indicated as

768 * for $p < 0.05$.

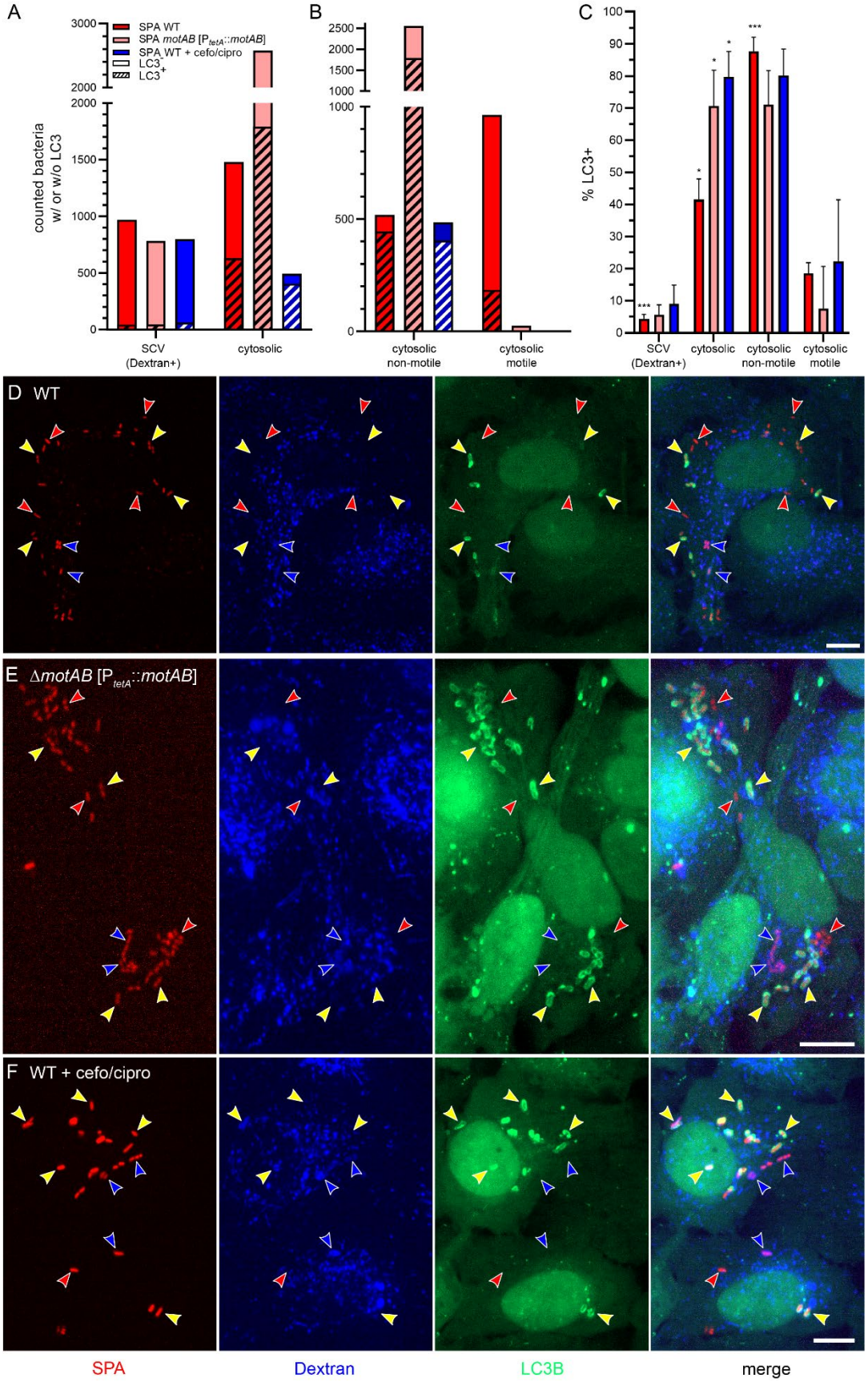
A
SPA WT
SPA motAB [PtetA::motAB]
SPA WT + cefo/cipro
LC3-
LC3+
counted bacteria w/ or w/o LC3
SCV (Dextran+)
cytosolic
B
cytosolic non-motile
cytosolic motile
C
% LC3+
SCV (Dextran+)
cytosolic
cytosolic non-motile
cytosolic motile
D WT
E ΔmotAB [PtetA::motAB]
F WT + cefo/cipro
SPA
Dextran
LC3B
merge

769

770 **Fig. 4. Cytosolic non-motile SPA are targeted by autophagosomal membranes. A-C.** HeLa
771 cells stably expressing LC3B-GFP (green) were pulse-chased with Dextran-Alexa647 (blue) and
772 infected with SPA WT or SPA Δ*motAB* [P_{tetA}::*motAB*] expressing mCherry (red) at MOI 30. 100
773 µg x ml^{-1} cefotaxime and ciprofloxacin were added to infected cells at 2 h p.i. if indicated. At 3-4
774 h p.i., randomly selected cells were imaged and later assessed for SPA associated with LC3B-
775 positive membranes. **A, B.** Total counts of SPA with (dashed bars) or without (bars) LC3B
776 decoration, compiled from three independent experiments. **B.** Cytosolic SPA quantified in **A** were
777 further scored as motile or non-motile, and assessed for LC3B decoration. **C.** Percentage of SPA
778 targeted by LC3B-containing membranes calculated from data shown in **A** and **B**. Data are means
779 and SD of 195 infected cells with 2,450 bacteria for WT, 171 infected cells with 3,360 bacteria for
780 Δ*motAB* [P_{tetA}::*motAB*], and 215 infected cells with 1,291 bacteria for WT + cefo/cipro from three
781 independent experiments. Statistical analysis was performed with one-way ANOVA and is
782 indicated as n.s., not significant; *, $p < 0.05$; **, $p < 0.01$; ***, $p < 0.001$. **D-F.** Representative
783 images showing subpopulations in SPA-infected cells. Arrowheads indicate SPA residing in SCV
784 (blue), cytosolic SPA (red), LC3B-decorated SPA (yellow). Images are shown as single Z-plane
785 from stack (**D**) or as maximum intensity projection (**E, F**). Scale bars: 10 µm.
786

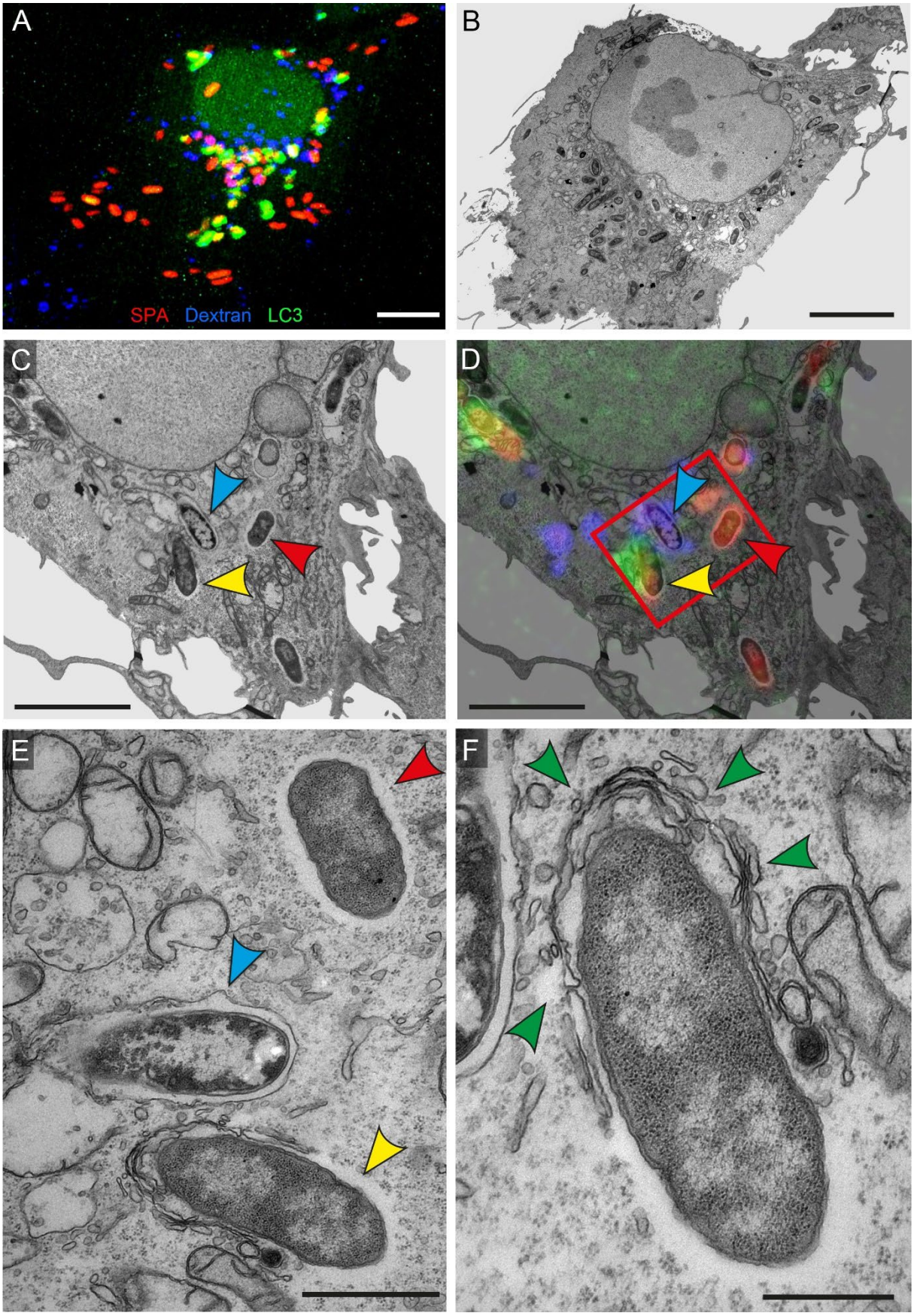

787

788 **Fig. 5. Various degrees of xenophagic capture of distinct subpopulations of intracellular SPA.**
789 HeLa cells expressing LC3B-GFP (green) were pulse-chased with Dextran-Alexa647 (blue) and
790 infected with SPA WT expressing mCherry (red) at MOI 30. Cells were fixed 4 h p.i. during LCI
791 (**A**), and subsequently processed for transmission electron microscopy (TEM) of ultrathin sections.
792 LCI and TEM images were superimposed for correlation (**D**) and details are shown at higher
793 magnification (**E**, **F**). Arrowheads indicate SPA residing in SCV (blue), cytosolic SPA (red) and
794 SPA targeted by LC3B-positive autophagosomal membrane (yellow). Partial enclosure by
795 autophagosomal membranes is indicated by green arrowheads. Scale bars: 10 µm (**A**, **B**), 5 µm (**C**,
796 **D**), 1 µm (**E**), 500 nm (**F**).

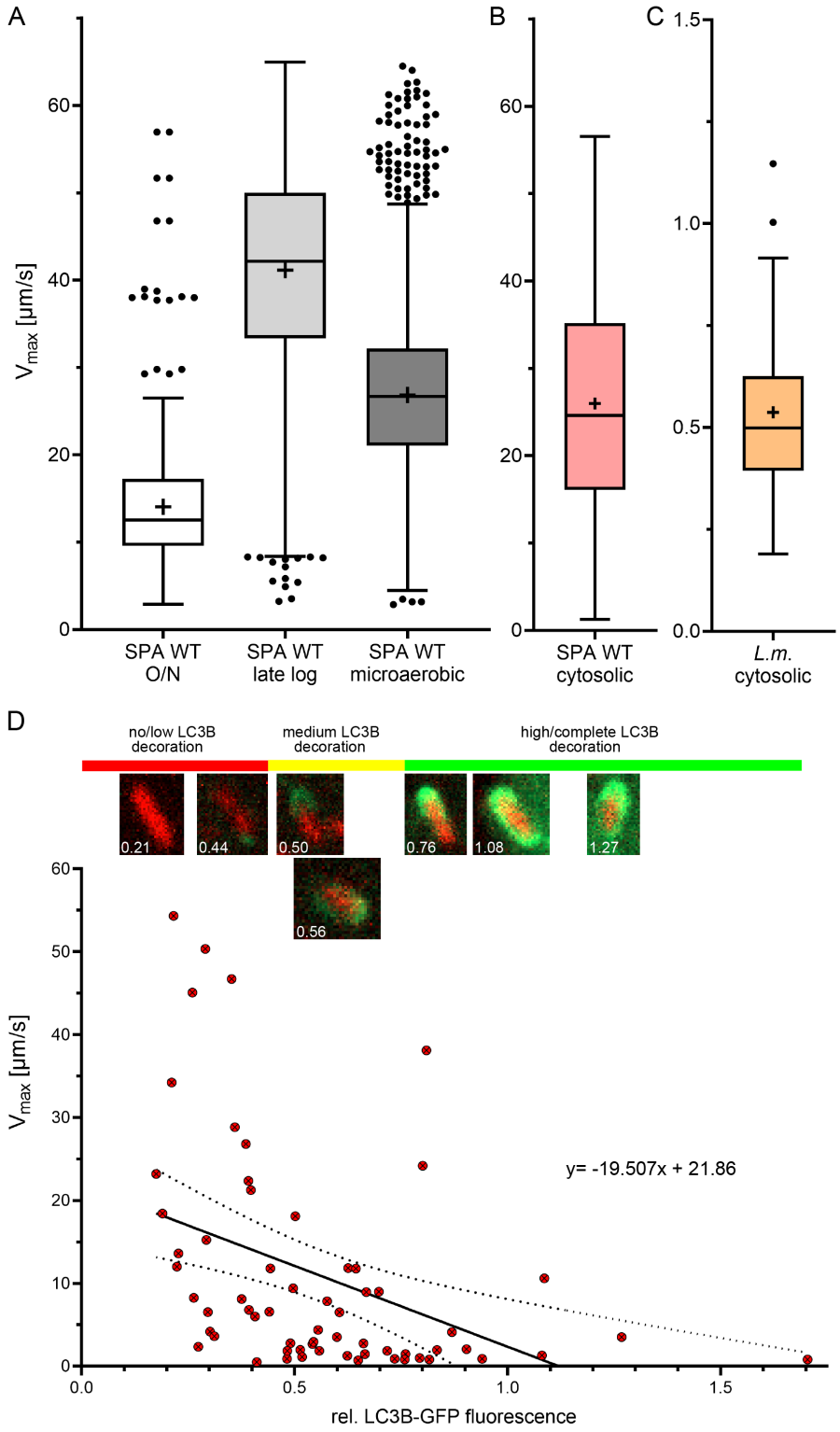

Fig. 6. Xenophagic capture reduces velocity of intracellular motile SPA. Single bacterial cells after culture in broth media (**A**), or within infected host cells (**B**, **C**) were registered by LCI.

800 Subsequently, bacterial motility was analyzed by automated (**A**, **C**) or manual (**B**) tracking
801 analyses. **A-C.** Maximum velocity of single bacterial cells from tracking SPA grown in culture
802 (**A**), or intracellular SPA (**B**) or *L.m.* (**C**). For single cell analyses, tracks of 476 SPA WT from O/N
803 culture, 7,058 SPA WT from late log culture, 2,998 SPA WT from micro-aerobic culture were
804 collected from one experiment. For intracellular bacteria, tracks of 16,248 cytosolic SPA WT were
805 collected from three independent experiments, and 42 tracks for *L.m.* from one experiment. Data
806 are shown as Tukey´s box plots with error bars including data of 1.5 x IQR. Outliers beyond the
807 1.5 x IQR are shown as dots. Middle line denotes median and "+" mean value. **D.** Plotting of SPA-
808 associated relative LC3B-GFP intensity against maximum velocity of individual cytosolic SPA.
809 Representative images from measurement of fluorescence intensity are shown as single Z-plane
810 from image stacks. Linear regression and 95% confidence bands were calculated for analyses of
811 63 cytosolic SPA from two independent experiments.
812

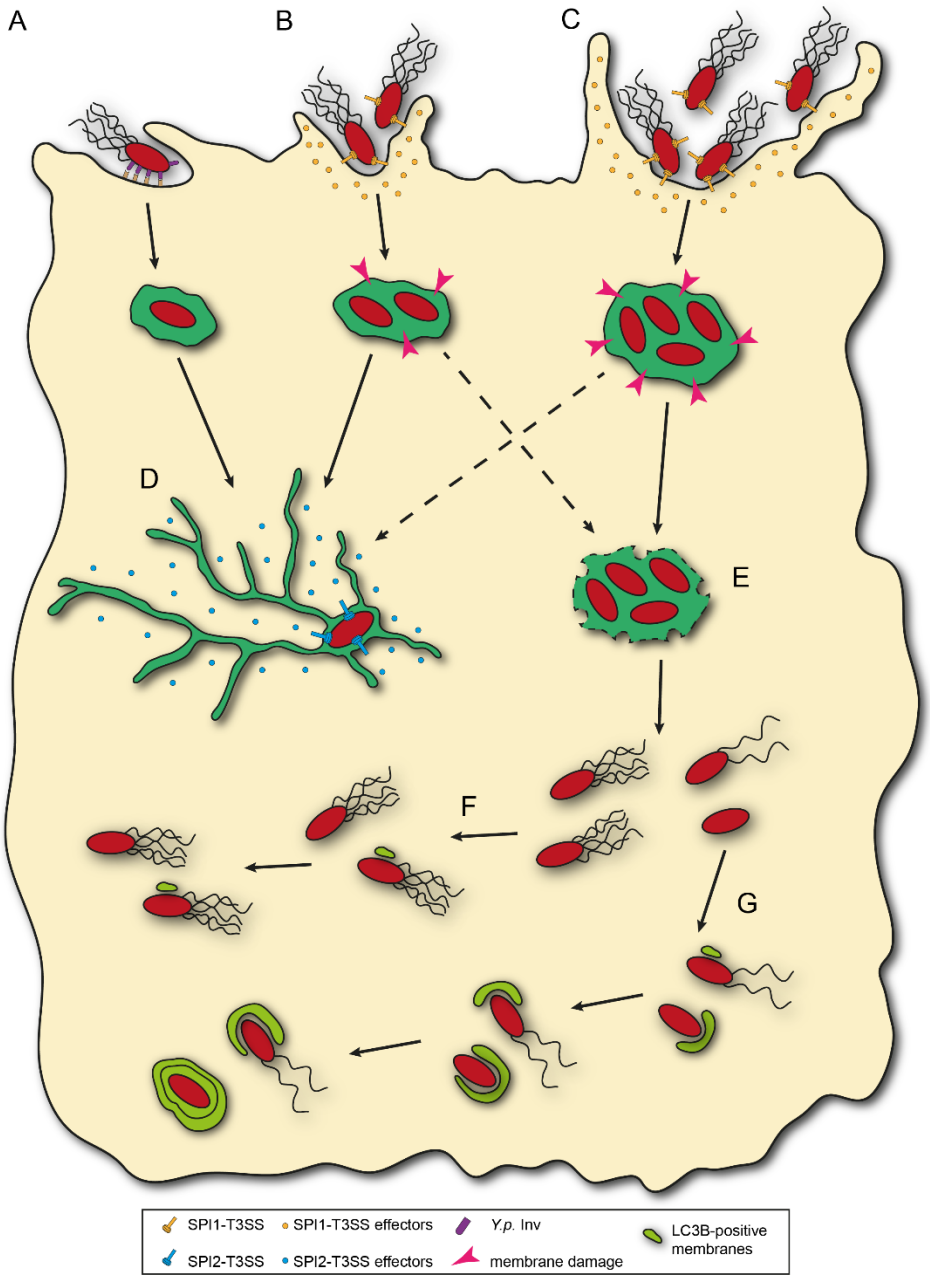

Fig 7. Model for SPA entry into host cell cytosol and autophagic decoration. Zipper or trigger invasion with limiting extend of membrane ruffling (**A**, **B**) primarily lead to an intracellular lifestyle with SCV maturation (**D**). Trigger invasion with extensive membrane ruffling and increased cooperative invasion (**C**) lead to membrane damage and rupture of the nascent SCV (**E**) and a cytosolic lifestyle of SPA. Flagellated and motile cytosolic SPA delay or escape xenophagic

819 capture (**F**). Non-motile cytosolic SPA are captured by LC3B-positive membranes, while flagella-
820 mediated motility permits evasion of xenophagy (**G**).

821

822 **Suppl. Tables**

823 **Table S1**. Oligonucleotides used in this study

Designation	Sequence 5' – 3'
Red mutagenesis	
sopE-Del-For	GGGCCGGGCAGTGTTGACAAATAAAGTCGTTAAAGATTTTGTGTAGGCTGGAGCTGCTTC
sopE-Del-Rev	AGGAAGAGGCTCCGCATATTTTTTGGTTTTTCAGTGTTCACATATGAATATCCTCCTTAG
sopE2-Red-Del-For	AAAGTGTAGCTATGCATAGTTATCTAAAAGGAGAACTACCGTGTAGGCTGGAGCTGCTTC
sopE2-Red-Del-Rev	TTAATTCATATGGTTAATAGCAGTATTGTATTTACTACCACATATGAATATCCTCCTTAG
MotA-Del13-For	CAACAGCGGAAGGATGATGTCGTGCTTATCTTATTAGGTTATTCCGGGGATCCGTCGACC
MotB-Del13-Rev	TTCCGCTTTTGGCGATGTGGGTACGCTTGCCGGCGGGGCTTGTAGGCTGGAGCTGCTTCG
uhpT Del13 For	CCATTCGCAGGTATAAAAATTAGCTCAGGAGTAATCCATGATTCCGGGGATCCGTCGACC
uhpT Del13 Rev	CGTTACCAAATGCACACATTTAAGCGATATTGACTTGCTGTGTAGGCTGGAGCTGCTTCG
Check PCR	
K2-red-del	CGGTGCCCTGAATGAACTGC
SopE-Delcheck-Rev	TTAGCACTGGTAAATGACGGTTTA
sopE2-ckeck-rev4	GCGTCGCCATAAAAACGAATA
MotB-Check-Rev	CCTGCAGAATAGTGAAGCCG
Q5SDM-ins-sfGFP-Rev	GCACCACACCGGTAAACA
Seq-For	CGCCAGGGTTTTCCCAGTCACGAC
MotA-Check-Rev	ATCATCGCCGTCATAAAATC

uhpT DelCheck For	GCTGTTGCCATTTCTGAACG
uhpT DelCheck Rev	ACAGGATGCCCATCATAACG
Gibson assembly	
Vf-p3776_5	GATCCTACGTACCCGGGAAAGAGGAGAAAAGTATGC
Vr-p4589_3	AGAAAATAATAAAAAAGCCGGATTAATAATCTG
1f-SPA-PsopE	GATTATTAATCCGGCTTTTTTATTATTTTCTCGGCCAGTGTACGTTCAA
1r-SPA-PsopE	TCCCGGGTACGTAGGATCGGTAATGATCCTTTTATATGTACATAAC
Vf-PtetA	TCCGGCGATTGATTCACCGAC
Vr-PtetA	TTCACTTTTCTCTATCACTGATAGGGAGTGGTA
1f-ptetA-SPAmotAB	CCCTATCAGTGATAGAGAAAAGTGAAGTGCTTATCTTATTAGGTTACCTGGT
1r-SPAmotAB-ptetA	GGTGAATCAATCGCCGGATCACCTCGGTTCCGCTTTTG

854 **Suppl. Figures and figure legends:**

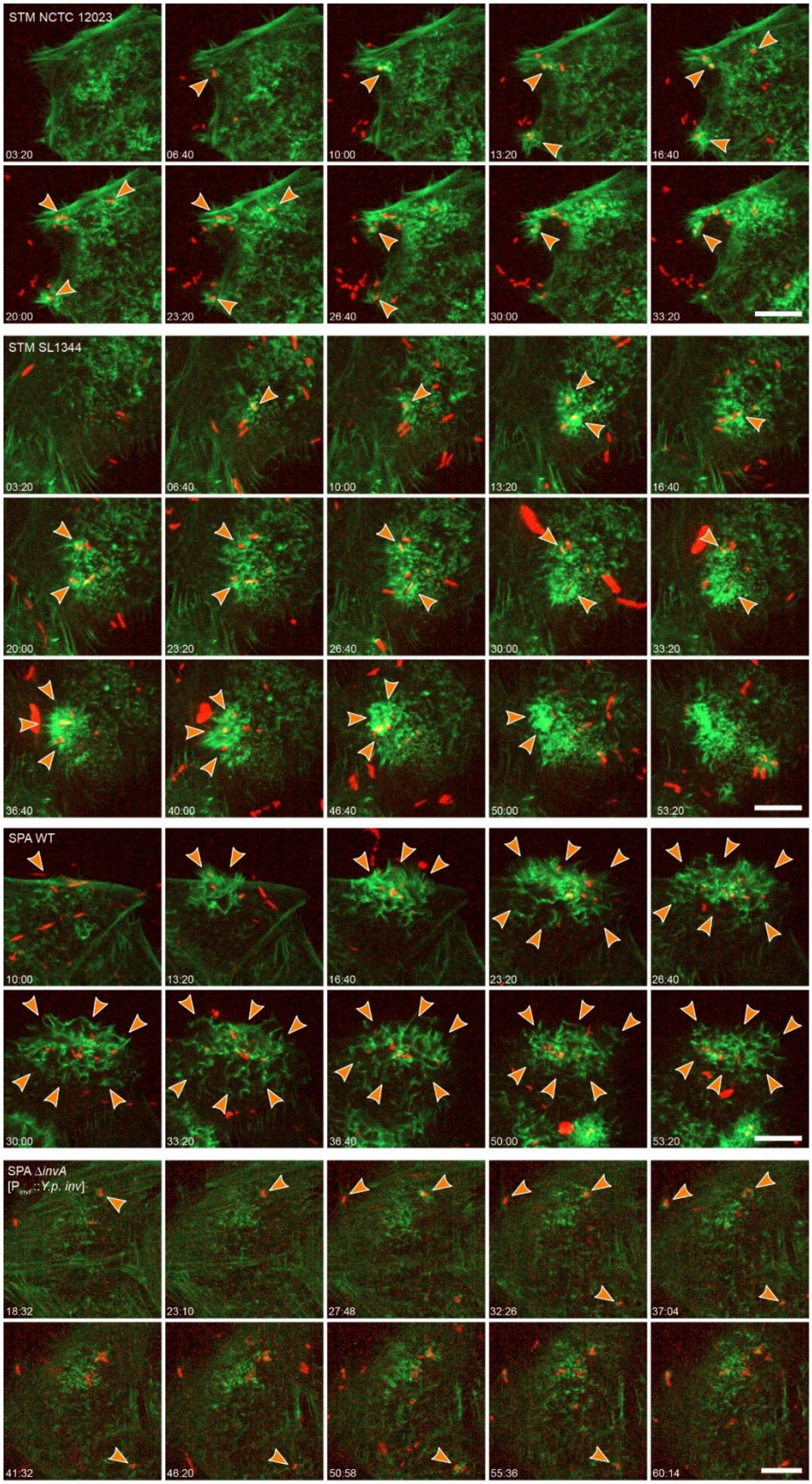

855

856 **Fig. S 1. SPA trigger invasion induces massive membrane ruffles and mediates highly**
857 **cooperative invasion.** HeLa cells stably expressing Lifeact-eGFP (green) were infected as
858 indicated with STM NCTC 12023, STM SL1344, SPA WT, or SPA Δ*invA* [P_{invF}::*Y.p. inv*]
859 expressing mCherry (red) at MOI 75. Cells were infected on microscope stage and imaged for
860 1 h by spinning disc confocal microscopy. Still images from representative time-lapse series
861 are shown, corresponding with the quantitative analyses shown in **Fig. 2**. Time stamp indicating
862 min:sec. Sites of ongoing invasion used for quantification of number of bacteria are indicated
863 by arrowheads. Scale bars: 10 µm.
864

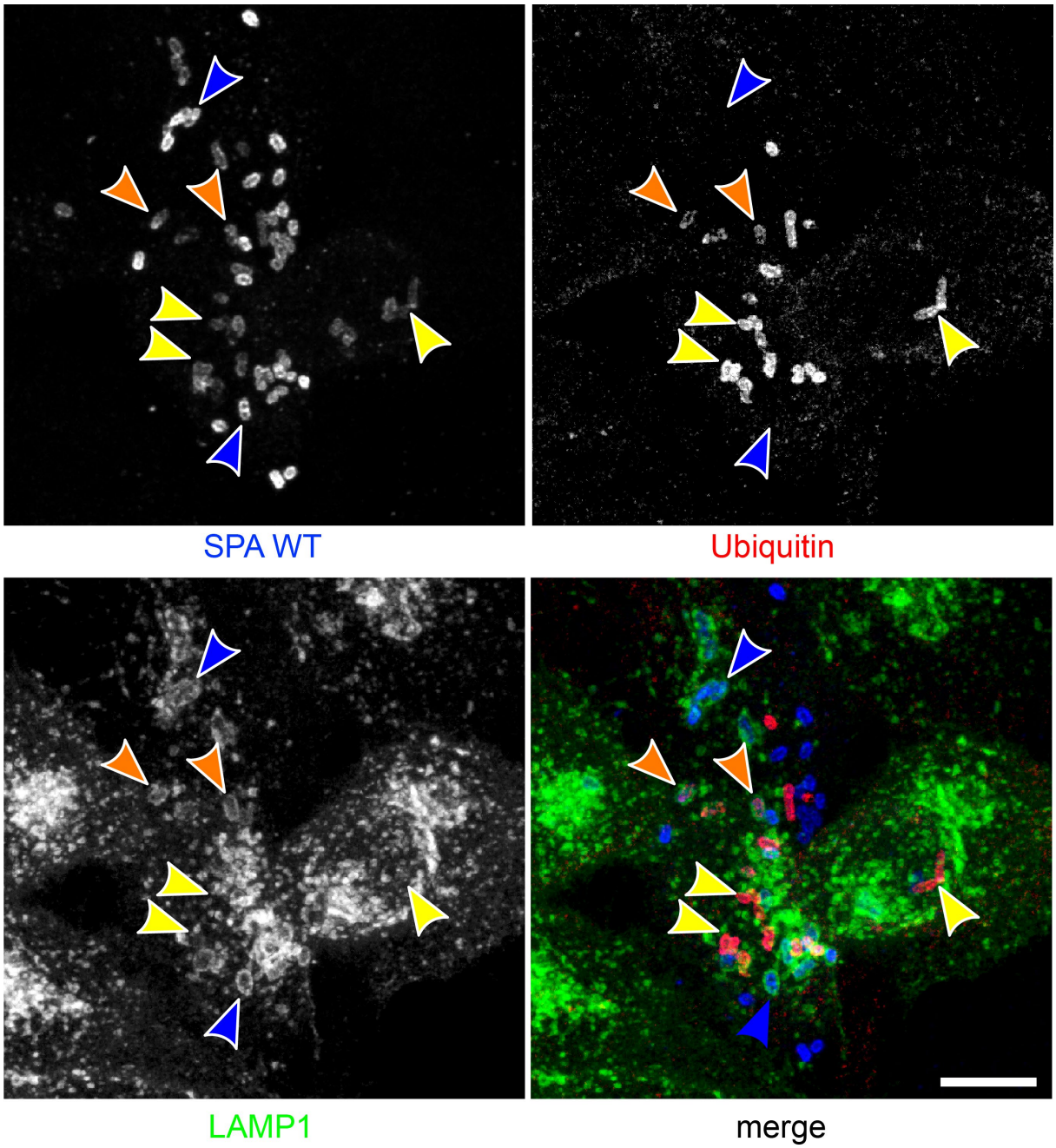

865

866 **Fig. S 2. Ubiquitylation of cytosolic SPA.** HeLa cells expressing LAMP1-GFP (green) were
867 infected with SPA WT at MOI 30. Cells were fixed at 7 h p.i. and immunolabeled for SPA LPS
868 (blue) and ubiquitin (red) prior to confocal microscopy. A representative maximum intensity
869 projection of an infected host cell is shown. Arrowheads indicate SPA in SCV without ubiquitin
870 signal (white), cytosolic SPA with ubiquitin signal (yellow), and SPA within partially intact
871 SCV and ubiquitin signal (orange), Scale bar: 10 µm.

872

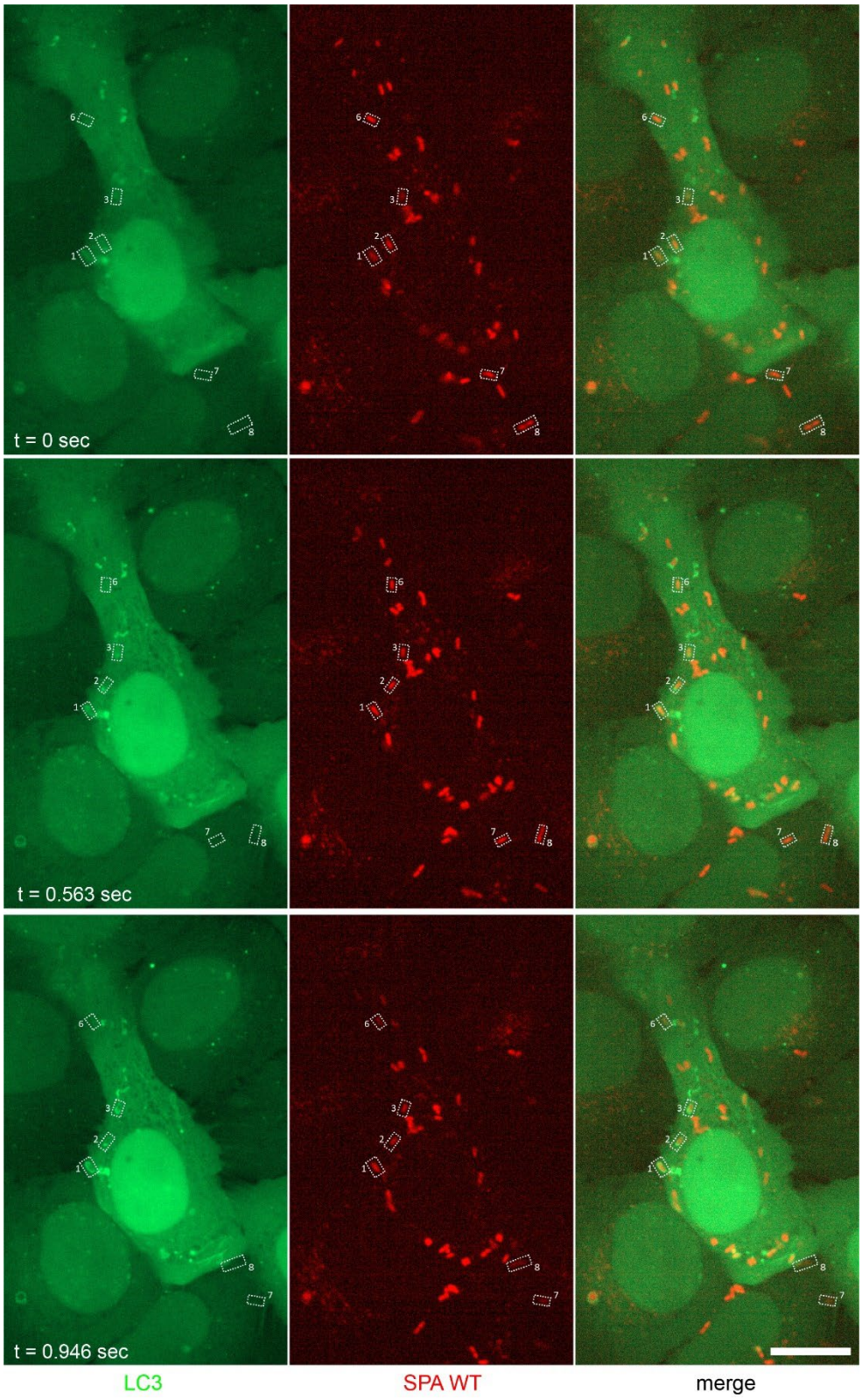

Fig. S 3. **Single cell quantification of LC3B-GFP fluorescence intensity and velocity of cytosolic SPA.** HeLa LC3B-GFP cells were infected with SPA WT expressing mCherry at MOI 30. At 3-4 h p.i. cells were imaged and cytosolic SPA were identified (boxes). For single SPA

877 cells LC3B-GFP fluorescence signal intensity was recorded, and velocity was determined by
878 single cell tracking. Three time points of a representative time lapse series are shown, and
879 quantitative data are displayed in **Fig. 6**. Images shown are single Z-planes from a stack. Scale
880 bar: 10 µm.
881

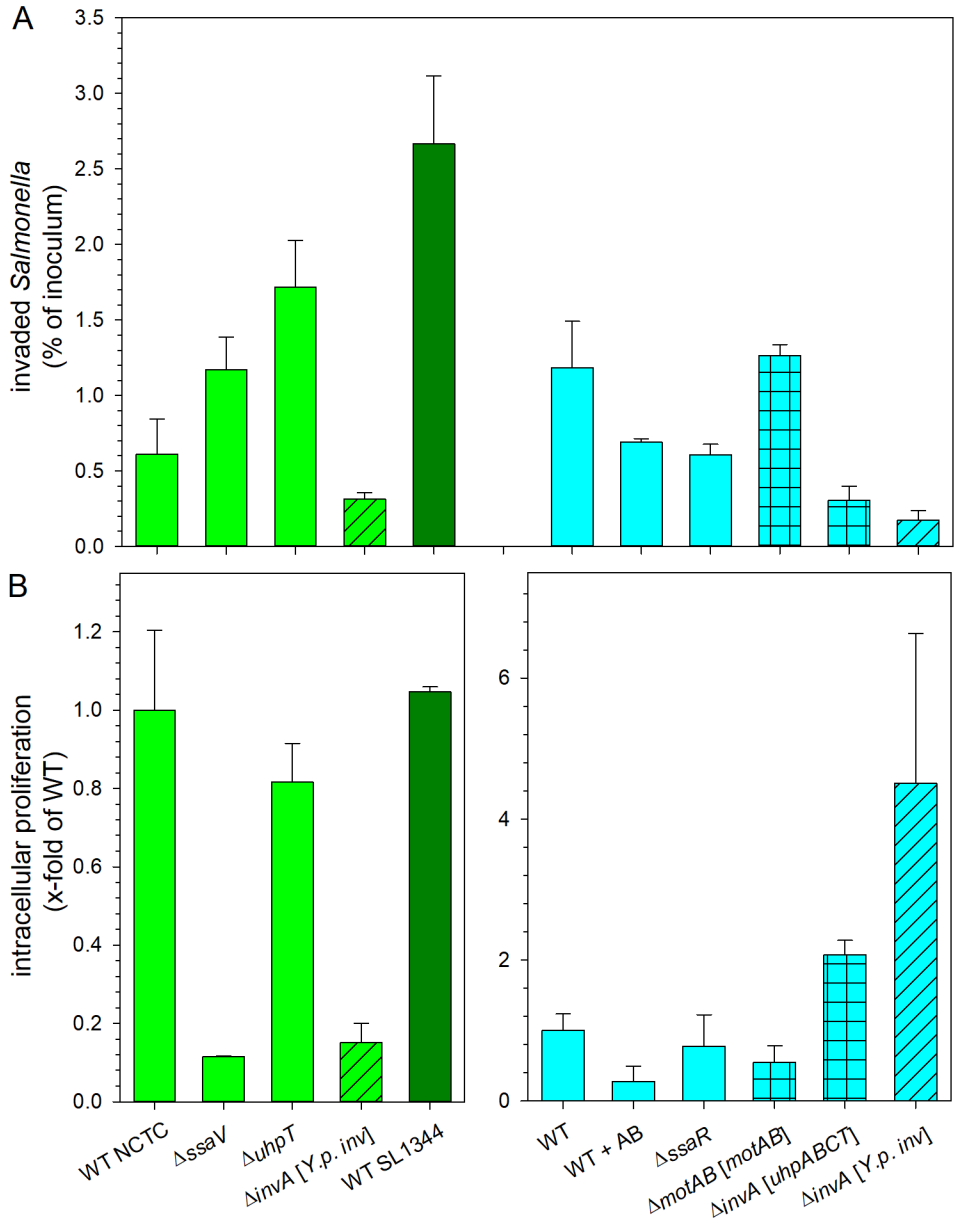

Fig. S 4. **Host cell invasion and intracellular replication of various STM and SPA strains.** HeLa cells were infected with STM (green) or SPA (cyan) WT or isogenic mutant strains at MOI 5. Presence of plasmids for expression *Y. pseudotuberculosis inv*, P_{tetA}::*motAB*, or STM *uhpABCT* is indicated by hatched bars. AB indicates addition of antibiotics cefotaxime and ciprofloxacin. Invasion (A) and intracellular replication (B) were determined by gentamicin protection assays comparing CFU counts of inoculum with lysates 1 h and 16 h p.i. Depicted are means and standard deviations of triplicate samples from one biological replicate performed.

891 **Suppl. Movie Captions**

892 **Movie 1: Live cell imaging of STM NCTC 12023 trigger invasion.** HeLa cells stably
893 expressing Lifeact-GFP (green) were infected with STM NCTC 12023 WT expressing mCherry
894 (red) and imaged over 1 h. The movie successively shows two individual clips. Time stamps in
895 upper corner indicates h:min:sec. Scale bar: 10 µm.

896 Link to movie: https://myshare.uni-osnabrueck.de/f/01372357bfbb44c49087/

897

898 **Movie 2**: **Live cell imaging of STM SL1344 trigger invasion.** HeLa cells stably expressing
899 Lifeact-GFP (green) were infected with STM SL1344 WT expressing mCherry (red) and
900 imaged over 1 h. The movie successively shows three individual clips. Time stamps in upper
901 corner indicates h:min:sec. Scale bar: 10 µm.

902 Link to movie: https://myshare.uni-osnabrueck.de/f/7c96d08641e24bc3b293/

903

904 **Movie 3: Live cell imaging of SPA WT trigger invasion.** HeLa cells stably expressing
905 Lifeact-GFP (green) were infected with SPA WT expressing mCherry (red) and imaged over 1
906 h. The movie successively shows two individual clips. Time stamps in upper corner indicates
907 h:min:sec. Scale bar: 10 µm.

908 Link to movie: https://myshare.uni-osnabrueck.de/f/62a3a98281dc496a9b04/

909

910 **Movie 4: Live cell imaging of SPA zipper invasion.** HeLa cells stably expressing Lifeact-
911 GFP (green) were infected with SPA *invA* [*Y.p. inv*] expressing mCherry (red) and imaged over

912 1 h. The movie successively shows three individual clips. Time stamps in upper corner indicates
913 h:min:sec. Scale bar: 10 µm.

914 Link to movie: https://myshare.uni-osnabrueck.de/f/5ae1904709b64a679b56/

915

916 **Movie 5**: **Live cell imaging of intracellular SPA WT targeted by LC3B.** HeLa cells stably
917 expressing LC3B-GFP (green) were infected with SPA WT expressing mCherry (red) and
918 imaged every two minutes over two hours. The movie successively shows three individual clips
919 with various degrees of xenophagic capture. Time stamps indicates minutes. Scale bar: 10 µm.

920 Link to movie: https://myshare.uni-osnabrueck.de/f/bbd7f3927781420382dc/

921

922 **Movie 6: Real-time imaging of intracellular SPA WT.** HeLa cells stably expressing LC3B-
923 GFP (green) were infected with SPA WT expressing mCherry (red) and pulse-chased with
924 Dextran AlexaFluor 647 (blue) if indicated, and imaged at frame rates of 2-3 frames per second.
925 Movie successively shows thee individual clips with various degrees of xenophagic capture.
926 Time stamps indicates seconds. Scale bar: 10 µm.

927 Link to movie: https://myshare.uni-osnabrueck.de/f/50d491e54e6a48c68c5a/